# Controlled DNA Patterning by Chemical Lift-Off Lithography: Matrix Matters

**Huan H. Cao,[†,‡] Nako Nakatsuka,[†,‡] Andrew C. Serino,[†,‡,§] Wei-Ssu Liao,[†,‡] Sarawut Cheunkar,[†,‡] Hongyan Yang,[∥] Paul S. Weiss,[*,†,‡,§] and Anne M. Andrews[*,†,‡,∥]**

[†]California NanoSystems Institute, University of California, Los Angeles, Los Angeles, California 90095, United States, [‡]Department of Chemistry and Biochemistry, University of California, Los Angeles, Los Angeles, California 90095, United States, [§]Department of Materials Science and Engineering, University of California, Los Angeles, Los Angeles, California 90095, United States, and [∥]Department of Psychiatry and Biobehavioral Health, Semel Institute for Neuroscience and Human Behavior, and Hatos Center for Neuropharmacology, University of California, Los Angeles, Los Angeles, California 90095, United States

**ABSTRACT** Nucleotide arrays require controlled surface densities and minimal nucleotide–substrate interactions to enable highly specific and efficient recognition by corresponding targets. We investigated chemical lift-off lithography with hydroxyl- and oligo(ethylene glycol)-terminated alkanethiol self-assembled monolayers as a means to produce substrates optimized for tethered DNA insertion into post-lift-off regions. Residual alkanethiols in the patterned regions after lift-off lithography enabled the formation of patterned DNA monolayers that favored hybridization with target DNA. Nucleotide densities were tunable by altering surface chemistries and alkanethiol ratios prior to lift-off. Lithography-induced conformational changes in oligo(ethylene glycol)-terminated monolayers hindered nucleotide insertion but could be used to advantage *via* mixed monolayers or double-lift-off lithography. Compared to thiolated DNA self-assembly alone or with alkanethiol backfilling, preparation of functional nucleotide arrays by chemical lift-off lithography enables superior hybridization efficiency and tunability.

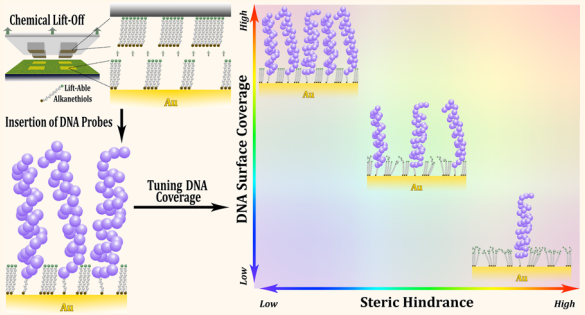


**KEYWORDS:** nucleotide arrays · chemical lift-off lithography · self-assembled monolayers · DNA hybridization · alkanethiol patterning

Nucleotide microarrays are widely used to identify specific DNA sequences and to investigate large-scale gene expression.[1] To fabricate arrays, probe nucleotides are immobilized on solid substrates for hybridization with complementary targets from solution. Tethering strategies include covalent binding, electrostatic interaction, biotin–streptavidin linkage, and thiolated nucleotide self-assembly.[2,3] Alkanethiol self-assembled monolayers (SAMs) on Au have been utilized to regulate surface-probe densities and probe-substrate interactions, thereby enhancing specific recognition of tethered DNA targets and minimizing nonspecific binding.[4−8] As such, the use of alkanethiol SAMs modified with DNA probes has advanced understanding of DNA-SAM and DNA–substrate interactions to improve and to optimize the performance of nucleotide-functionalized substrates.[9−15]

Tarlov *et al.* illustrated the importance of alcohol-terminated alkanethiols on Au substrates to facilitate target DNA hybridization.[4,16,17] Here, alkanethiol-DNA was self-assembled and then backfilled with mercaptohexanol (MCH) to dilute the DNA and to prevent direct interactions between DNA probes and substrates.[4,18] Backfilling with alkanethiols also lowers quenching of fluorescently labeled DNA by preventing DNA molecules from lying flat on metal substrates.[12,19] In addition to MCH, mercaptoundecanol (MCU) and oligo(ethylene glycol)-terminated alkanethiols have been used as diluents.[6,7,20−22] The presence of the latter reduces nonspecific interactions with proteins and other biomolecules.[9,23,24] For example, Choi *et al.* demonstrated that DNA substrates created by backfilling with hydroxyl- and carboxyl-terminated oligo(ethylene glycol)-containing alkanethiols and functionalized with cell-adhesion peptides

* Address correspondence to aandrews@mednet.ucla.edu, psw@cnsi.ucla.edu.

Received for review September 3, 2015 and accepted October 1, 2015.

**Published online October 01, 2015**
**10.1021/acsnano.5b05546**

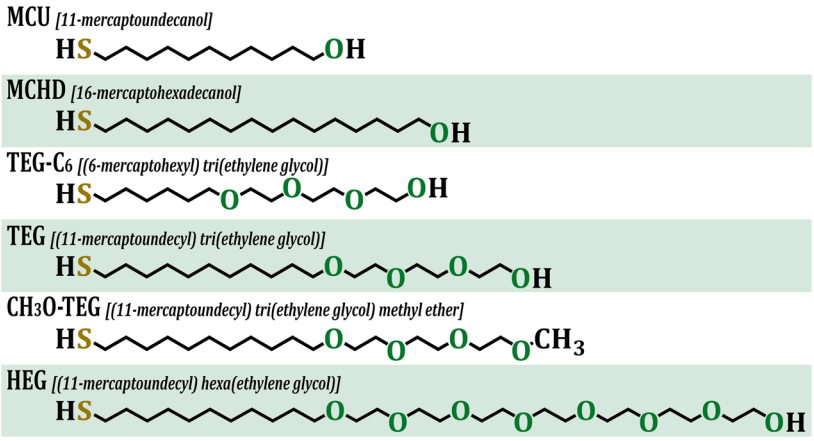


**Scheme 1. Abbreviations, names, and molecular structures of the alkanethiols used in these studies.**

simultaneously promoted peptide-selective cell adhesion and DNA hybridization.[25]

In lieu of backfilling, thiolated DNA can be inserted into preformed alkanethiol SAMs.[6,26,27] Insertion is advantageous for a number of reasons. Instead of exposing surface-bound DNA to ethanolic alkanethiol solutions during backfilling, which causes DNA condensation and precipitation, alkanethiols are assembled first followed by insertion of DNA dissolved in aqueous buffers.[28,29] Insertion also prevents phase separation.[23,30−33] A recent study of DNA hybridization on Au electrodes demonstrated that surface hybridization was reduced because DNA probes tended to aggregate into domains after backfilling with alcohol-terminated alkanethiols.[34] In contrast, tethered DNA molecules inserted into defect sites in preformed SAMs produced dilute coverage wherein individual probe strands were isolated from each other.[34,35] A low-density environment for surface-bound DNA not only improves hybridization by providing better access for target DNA but it enables investigation of DNA−substrate interactions at the single-molecule level.[34−37]

Insertion-directed chemistries are also beneficial because they can be combined with surface patterning methods.[38−40] We developed microcontact insertion printing for substrate patterning[38] and have used this technique to produce dilute coverage of surface-tethered small-molecule ligands on preformed oligo(ethylene glycol)-terminated alkanethiol SAMs.[23] However, using microcontact insertion printing for DNA patterning will require tuning stamp surface chemistries to facilitate insertion of alkanethiol-functionalized DNA into SAMs.[41] Alternately, we illustrate how patterning characterized by dilute DNA surface coverage and reduced DNA−substrate interactions can be achieved straightforwardly using chemical lift-off lithography.[42] Lift-off lithography takes advantage of the strong interactions formed during stamp-substrate contact between the siloxyl groups on oxygen plasma-treated polydimethylsiloxane (PDMS) stamps and hydroxyl-terminated alkanethiol SAMs. Boxer and co-workers have used similar strategies to remove molecules from lipid bilayers.[43−45] In lift-off lithography, terminally ($\omega$-) functionalized alkanethiol molecules are removed when stamps are lifted from substrates. Here, we investigated how retained alkanethiols in the contacted regions interact with DNA probes to modulate surface properties. A range of alkanethiols terminated with hydroxyl or oligo(ethylene glycol) functional groups were studied (Scheme 1).

We find that following lift-off lithography, hydroxyl-terminated alkanethiol SAMs enable DNA probes greater access to Au substrates compared to oligo(ethylene glycol)-terminated SAMs. Notably, alkanethiol-functionalized DNA inserted into post-lift-off hydroxyl-terminated alkanethiol SAMs showed increased surface hybridization compared to DNA monolayers assembled by backfilling. Moreover, alkanethiol backfilling following patterning *via* lift-off lithography did not improve DNA hybridization efficiency. We discovered that the lift-off process induces conformational changes in oligo(ethylene glycol) moieties resulting in steric effects that limit DNA-probe access to Au surfaces. As such, we varied hydroxyl-/oligo(ethylene glycol)-terminated alkanethiol SAM ratios *via* codeposition prior to lift-off to tune the amounts of inserted tethered DNA. Ultimately, chemical lift-off lithography, in combination with variable matrix compositions, provides a facile means to regulate and to optimize DNA surface coverage, which is essential for controlling hybridization efficiency and the thermodynamic/kinetic behavior of nucleic acids on surfaces.[5,46,47]

## RESULTS

**Chemical Lift-Off Lithography Facilitates Probe DNA Insertion and Target DNA Hybridization.** Following self-assembly, oxygen-plasma-treated PDMS stamps were used to remove alkanethiols terminated with hydroxyl moieties from Au substrates within the stamp-substrate contact areas.[42] Previously, we found that ~70% of MCU molecules are removed from the contact regions after lift-off.[42] Further, we showed that inserting biotin

hexa(ethylene glycol)-terminated alkanethiols into the contact areas enabled streptavidin recognition in the biotin-patterned regions with features as small as 40 nm for a single lift-off step and 20 nm for two lift-off lithography steps. The precision of these features reached 2 nm and later results showed that we have not yet reached the resolution limits of the method. Similarly, we reasoned that alkanethiol residues remaining in the contact areas after lift-off would act as diluents when inserting thiolated single-stranded DNA probes.

The chemical lift-off process is illustrated in Figure 1. Negative features in SAMs were generated using PDMS stamps with arrays of protruding square-shaped posts. Patterned SAMs were incubated with alkanethiol-functionalized DNA probe solutions to enable insertion into the post-lift-off areas. Substrates were then exposed to fluorescently labeled target DNA. Experiments were carried out using ~17 h (overnight) insertion times. Short insertion times (*i.e.*, <2 h) were associated with linearly increasing hybridization efficiencies, whereas DNA insertion over longer times resulted in near saturation of hybridization efficiency (Figure S1).

A representative fluorescence image of a DNA array formed on a patterned MCU SAM following hybridization with complementary DNA is shown in Figure 2A. Specificity of target DNA hybridization is indicated by the lack of a fluorescence pattern when a similar substrate was challenged with noncomplementary target DNA (Figure 2B). The DNA arrays on post-lift-off tri(ethylene glycol)-terminated undecanethiol (TEG) SAMs showed faint yet discernible fluorescent patterns compared to MCU SAMs (Figure 2C) and similarly lacked detectable fluorescence when hybridized with noncomplementary target DNA (Figure 2D). These results illustrate that hydroxyl-terminated (MCU) and tri(ethylene glycol)-terminated (TEG) molecules in the lift-off regions act as diluting matrices to enable tethered DNA probe insertion and specific hybridization with target DNA, albeit with different efficiencies.

Prior infrared spectral analysis indicated ~70% lift-off yields for MCU.[42] Here, we compared lift-off efficiencies for MCU *vs* TEG, which were not significantly different (MCU 64 ± 7% *vs* TEG 73 ± 2%; $N = 3$; $t(4) = 1$; $P > 0.05$). Thus, DNA insertion into post-lift-off MCU and TEG SAMs was anticipated to occur at similar levels. Nonetheless, fluorescence signals from DNA surface hybridization on TEG SAMs were substantially lower than those detected on MCU SAMs (Figure 2E).

We have used sequential lift-off steps to produce substrate features smaller than actual stamp features in doubly contacted regions.[42] Here, we employed double lift-off lithography to investigate whether additional TEG molecules could be removed from SAM substrates to improve DNA insertion and hybridization. First, flat stamps were used to lift-off TEG across entire substrates. Patterned PDMS stamps were next employed

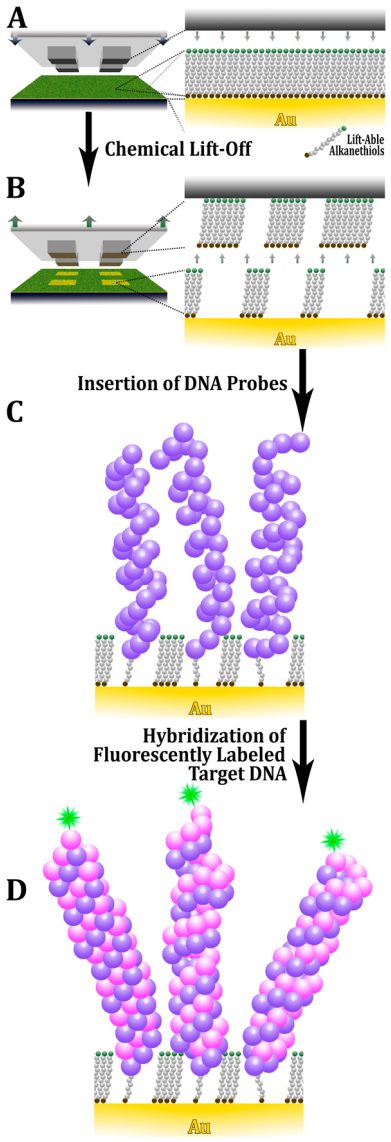


**Figure 1. Schematic illustration of chemical lift-off/DNA-insertion patterning. (A) Oxygen plasma-treated polydimethylsiloxane stamps are brought into conformal contact with alkanethiol self-assembled monolayers (SAMs) terminated with functional groups that are reactive toward chemical lift-off. (B) As a result of the strong interactions at stamp-substrate interfaces, stamp removal causes lift-off of functionalized alkanethiols, albeit incompletely, from Au substrates. (C) The exposed lift-off regions are then insertion-functionalized with alkanethiol-functionalized DNA probes, (D) followed by surface hybridization with fluorescently labeled target DNA.**

to remove additional TEG molecules only in the regions contacted by the stamp features. Alkanethiol probe DNA was then inserted followed by exposure to either fully complementary (Figure 2F) or noncomplementary (Figure 2G) fluorescently labeled target DNA. Hybridization was specific and greater DNA insertion and/or surface hybridization occurred on post-double-lift-off TEG SAMs compared to post-single-lift-off TEG SAMs (Figure 2E). Patterned fluorescence intensities after double lift-off lithography were twice those following single lift-off (Figure 2E) and notably, are the

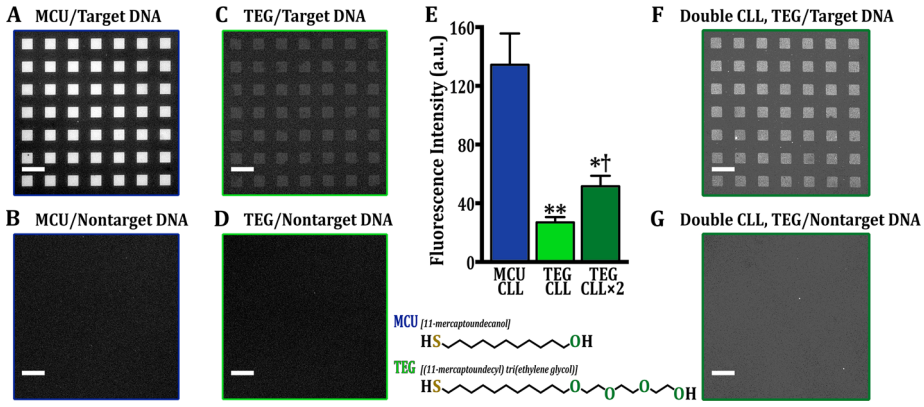


**Figure 2. Representative fluorescence images displaying (A,C,F) hybridization of surface-bound DNA probes (34 bases) with fluorescently labeled complementary target DNA or (B,D,G) hybridization with noncomplementary DNA (scrambled 34-base sequences). Post-lift-off self-assembled monolayers (SAMs) are (A,B) hydroxyl-terminated alkanethiols (MCU) or (C,D,F,G) tri(ethylene glycol)-terminated (TEG) alkanethiols. The fluorescence patterns in (F,G) represent double lift-off regions against a post-single-lift-off background. Fluorescence patterns in (A,C,F) compared to their absence in (B,D,G) indicate specific hybridization between Alexa Fluor 488-labeled target DNA (excitation at 495 nm) and tethered probe DNA. (E) Patterned specific fluorescence intensities resulting from DNA hybridization on post-lift-off MCU SAMs were higher than those observed on post-lift-off TEG SAMs. (F) Patterned specific fluorescence intensity was increased on post-double-lift-off TEG SAMs. Fluorescence images were taken with the same exposure times of 5 s at an emission wavelength of 517 nm. Stamp features are (25 $\mu$m × 25 $\mu$m). Error bars represent standard errors of the means with $N = 3$ samples per group. Mean intensities were significantly different across groups [$F(2,6) = 18$; $P < 0.01$]. *$P < 0.05$ and **$P < 0.01$ *vs* MCU/CLL; †$P < 0.05$ *vs* TEG/CLL. Scale bars are 50 $\mu$m.**

differences between DNA hybridization in post-double-lift-off regions *vs* the single-lift-off background.

**Oligo(Ethylene Glycol)-Terminated Alkanethiols Reduce DNA Insertion.** The findings in Figure 2 suggest that ethylene glycol moieties in TEG hinder the numbers of tethered DNA probes inserted into the lift-off regions of patterned substrates. Alternately, the flexible ethylene glycol segments might interfere with tethered probe DNA surface orientations so as to disfavor hybridization. Both scenarios could lower hybridization efficiency. Several studies have found that although oligo(ethylene glycol)-terminated alkanethiols are longer than comparable hydroxyl-terminated alkanethiols, the ethylene glycol moieties do not interfere with DNA orientations favorable for surface hybridization.[6,21,22,25] In light of this understanding and the double-lift-off findings above, we posited that the ethylene glycol moieties in TEG reduce DNA access to post-lift-off regions during insertion thereby lowering DNA-probe surface densities.

To test this hypothesis, thiolated DNA inserted into post-lift-off hydroxyl-terminated (MCU) *vs* tri(ethylene glycol)-terminated (TEG) SAMs was compared using atomic force microscopy (AFM). After lift-off, MCU and TEG SAMs displayed similar negative-height topographic features where PDMS stamps had contacted SAMs (Figure 3A,B, respectively). Following incubation with DNA probes, positive-height topographic features protruding beyond SAM backgrounds were observed for MCU SAMs (1.5 ± 0.06 nm, Figure 3C), indicating that DNA had been inserted. Significantly smaller height increases were observed for DNA inserted on TEG SAMs (0.34 ± 0.02 nm, [$t(8) = 19$; $P < 0.001$], Figure 3D) suggesting that fewer DNA probe molecules had been inserted compared to MCU SAMs.

Although we observed differences in AFM topographic heights between thiolated DNA inserted into post-lift-off MCU *vs* TEG SAMs, height differences alone do not conclusively indicate that fewer DNA probes were present on post-lift-off TEG SAMs. Because TEG molecules are longer than MCU molecules by three ethylene glycol units, upon insertion, the observed height difference between DNA molecules and the TEG SAM background is expected to be smaller than that observed with the MCU SAM background. Additional AFM experiments were carried out using longer thiolated single-stranded DNA probes (100 bases) to increase AFM topographic contrast over insertion of 34-base DNA probes. An increase in height was observed on post-lift-off MCU SAMs indicating insertion of long DNA probes (2.1 ± 0.07 nm, Figure 3E). Observable, yet smaller height increases were found for post-lift-off TEG SAMs (0.78 ± 0.05 nm, Figure 3F). Mean topographic heights of MCU/DNA SAMs were again significantly different from TEG/DNA SAMs [$t(6) = 16$; $P < 0.001$].

The apparent height differences between the patterned and unpatterned regions in Figure 3F substantiate DNA-probe insertion on TEG SAMs. However, similar to short DNA, differences in AFM topographic heights where long DNA was inserted into post-lift-off MCU (Figure 3E) *vs* TEG SAMs (Figure 3F) might still be due to the smaller height differences between DNA molecules and TEG *vs* MCU molecules. Assuming a 0.34 nm distance between DNA bases,[48] fully extended 34- and 100-base single-stranded DNA molecules would be ~12 and 34 nm long, respectively. The protruding features on post-lift-off MCU and TEG SAMs (Figure 3C,D,E,F) are substantially smaller than the

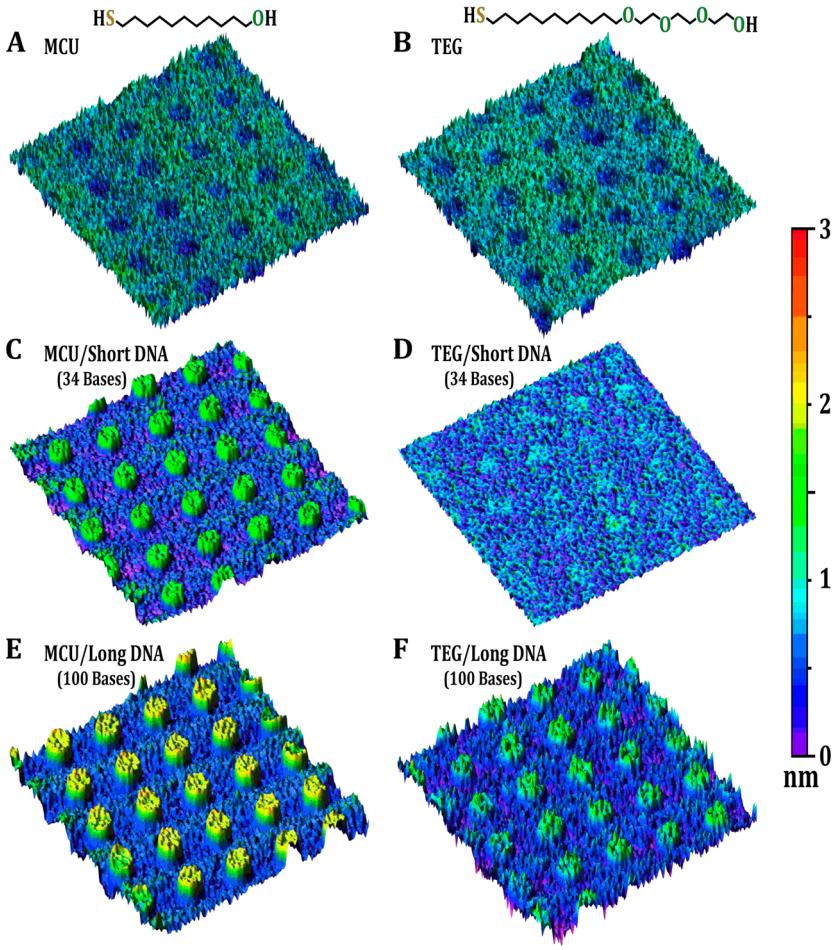


**Figure 3. Atomic force microscopy images before and after insertion with short or long DNA. Negative SAM features resulting from chemical lift-off of (A) hydroxyl-terminated alkanethiol self-assembled monolayers (SAMs) or (B) tri(ethylene glycol)-terminated SAMs indicate similar degrees of lift-off. After short (34-base) or long (100-base) thiolated DNA was inserted into the lift-off areas, protruding features were observed on MCU SAMs (C,E), while lower-contrast DNA features appeared on TEG SAMs (D,F). Differences in topographic heights between (C) *vs* (D) and (E) *vs* (F) suggest that fewer DNA probe molecules were inserted into the post-lift-off areas of TEG SAMs, regardless of DNA length. Images are representative of $N = 4-5$ samples per condition. Image dimensions are 20 $\mu$m $\times$ 20 $\mu$m.**

extended DNA lengths. Since AFM images were collected under dry conditions and the DNA molecules constitute only a fraction of each monolayer, the segments of the inserted DNA that lay beyond the matrices were unlikely to be fully extended. Thus, the relative height differences observed on post-lift-off MCU *vs* TEG SAMs do not reflect absolute DNA heights relative to SAMs but instead, indicate relative differences in the numbers of inserted molecules. Below, we use these results to estimate the fractions of monolayers associated with inserted DNA. Beyond these estimates, any potential effects of DNA probe lengths on insertion efficiency into SAMs[49] cannot be straightforwardly differentiated by AFM.

**Chemical Lift-Off Reduces DNA–Substrate Interactions and Improves DNA Hybridization.** We used X-ray photoelectron spectroscopy (XPS) to quantify DNA-associated nitrogen and phosphorus signals on MCU *vs* TEG patterned surfaces. Since we were interested in probe DNA inserted into post-lift-off regions, featureless PDMS stamps were used with chemical lift-off lithography for these experiments to maximize lift-off areas. In addition, because we focused on investigating the XPS fingerprints of DNA, only the N 1s and P 2p XPS data are discussed here. The complete XPS data can be found in the Supporting Information (Table S1). The bottom curves in Figure 4 indicate that N 1s and P 2p peaks were not present on post-lift-off MCU and TEG SAMs in the absence of DNA probes (*i.e.*, incubation with 0.01 M phosphate-buffered saline), as expected. Both N 1s and P 2p peaks corresponding to 6.9 atomic % and 2.0 atomic %, respectively (Table 1), were observed for thiolated DNA inserted into post-lift-off MCU SAMs (lower-middle curves, Figure 4A,C). By contrast, these peaks were undetectable for DNA inserted into post-lift-off TEG SAMs (middle curves, Figure 4B,D).

The absence of nitrogen and phosphorus peaks associated with post-lift-off TEG SAMs suggests that DNA insertion into post-lift-off TEG SAMs was either absent or below the XPS detection limit. We conclude

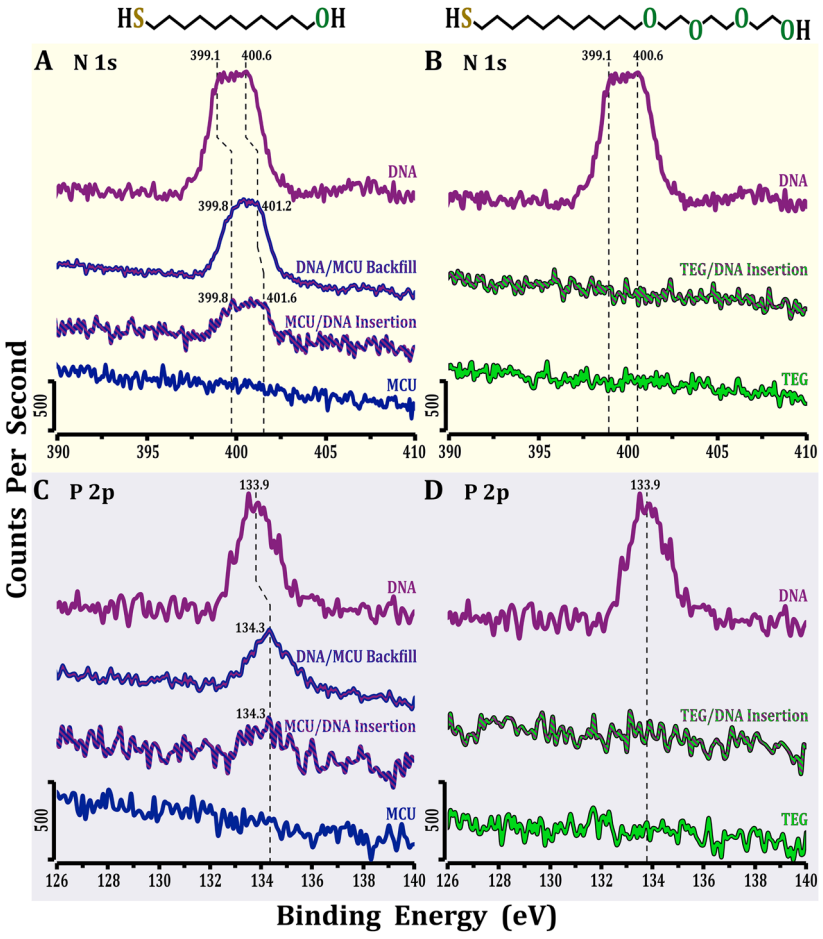


**Figure 4. Representative X-ray photoelectron spectra of N 1s and P 2p peaks associated with (A,C) hydroxyl-terminated (MCU) and (B,D) tri(ethylene glycol)-terminated (TEG) alkanethiol self-assembled monolayers (SAMs). All bottom curves represent post-lift-off SAMs incubated with 0.01 M phosphate buffered saline devoid of thiolated DNA probes, hence the absence of nitrogen and phosphorus peaks in these curves. The large N 1s and P 2p peaks from pure DNA monolayers (all top curves) are in contrast to the smaller peaks (all middle curves) from MCU/DNA and TEG/DNA mixed SAMs indicating dilute DNA coverage on MCU-backfilled (upper middle curves A,C) and post-lift-off MCU (lower middle curves A,C) SAMs. The apparent shift to lower energies in N 1s (~0.6−1 eV) and P 2p (~0.4 eV) peaks on pure DNA SAMs compared with alkanethiol/DNA SAMs is attributed to greater DNA−substrate interactions associated with the pure DNA SAMs. Spectra are displaced vertically for ease of visualization.**

the latter case is correct in light of the detectable fluorescence microscopy patterns (Figure 2C) and AFM topographies (Figure 3D,F) on similar substrates. Consequently, XPS may not be sensitive enough to detect small amounts (≤1% monolayer, *vide infra*) of DNA-associated nitrogen and phosphorus on post-lift-off TEG SAMs.

The broad N 1s peak for DNA on post-lift-off MCU SAMs (lower-middle curve, Figure 4A) arises from nitrogen peaks associated with heteroaromatic DNA nitrogen at 399.8 eV, and C(═O)—N, N—C(═O)—N and C(═O)—N—C(═O) moieties at 401.6 eV.[50] These nitrogen peaks were at higher binding energies (~1 eV) in comparison to undiluted tethered DNA monolayers (top *vs* lower middle curves in Figure 4A). Previous studies have shown that heteroaromatic nitrogen in undiluted DNA monolayers interacts with Au substrates, resulting in lower N 1s binding energies compared to the same nitrogen species in DNA bases that are free from substrate interactions.[7,21,51] Additionally, the P 2p peaks from post-lift-off MCU/DNA SAMs were at a higher binding energy (~0.4 eV) than for pure DNA monolayers (top *vs* lower middle curves, Figure 4C). Nitrogen and phosphorus XPS peaks shifted to higher energies indicate that DNA base-substrate interactions are reduced in the presence of post-lift-off MCU molecules suggesting that DNA bases are more available to hybridize with complementary bases in target DNA. In contrast, the thiolated DNA molecules in pure DNA monolayers tend to lie down on metal surfaces such that bases interact with Au substrates disfavoring hybridization with target DNA.

We also prepared substrates using the backfilling method wherein thiolated DNA SAMs were subsequently exposed to MCU solutions (upper-middle curves, Figure 4A,C). Backfilling was carried out for 30 min because previous studies showed that this incubation time results in DNA-probe orientations that

favor hybridization.[7] Similar to DNA inserted in post-lift-off MCU SAMs, nitrogen and phosphorus XPS peaks were at higher binding energies (~0.4 eV for N 1s and ~0.6 eV for P 2p) for MCU-backfilled DNA SAMs compared to undiluted DNA monolayers indicating reduced DNA base-substrate interactions.

Prior studies have shown that differences in N 1s and P 2p binding energies between undiluted DNA monolayers and DNA/alkanethiol SAMs not only indicate reduced DNA−substrate interactions in the latter but also upright orientation of DNA probes.[7,15,21] For example, near-edge X-ray absorption fine-structure spectroscopy has been used to show that shifts to higher binding energies for the N 1s and P 2p XPS signals associated with DNA/alkanethiol monolayers are accompanied by upright probe orientations on Au surfaces.[7,21,52] The N 1s and P 2p peak areas (Table 1) from post-lift-off MCU/DNA SAMs (6.9 atomic % nitrogen and 2.0 atomic % phosphorus) *vs* those of MCU-backfilled DNA SAMs (13.2 atomic % nitrogen and 3.1 atomic % phosphorus) and undiluted DNA monolayers (15.6 atomic % nitrogen and 3.6 atomic % phosphorus (Figure 4A,C) indicate lower surface coverages of DNA probes on post-lift-off MCU SAMs. Compared with pure DNA monolayers, DNA probes are diluted by ~50% on post-lift-off MCU SAMs, in agreement with previous studies.[6,7,21] These surface coverage estimates, however, are only relative because XPS signals are affected not only by the numbers of molecules on the substrates but also by X-ray attenuation lengths.[51]

Since the XPS data in Figure 4 show that various methods result in different amounts of surface-assembled DNA, we investigated whether this translated into differential DNA hybridization. Fluorescence resulting from target DNA hybridization on substrates prepared using lift-off lithography followed by probe-DNA insertion was significantly greater than fluorescence intensities from hybridization on undiluted DNA monolayers (Figure 5A). Moreover, there was greater fluorescence on post-lift-off MCU SAMs compared to MCU-backfilled DNA SAMs. Considering that post-lift-off MCU SAMs had the *lowest* numbers of DNA probe molecules compared to pure DNA monolayers and MCU-backfilled DNA SAMs (Table 1 and Figure 4A,C), these results indicate improved DNA hybridization efficiency associated with the chemical lift-off lithography-DNA insertion approach (Figure 5B), in agreement with studies using other insertion methods.[34,35] Notably, the coefficients of variation (%CV) for hybridization were significantly lower for the lift-off-insertion approach signifying improved reproducibility (Figure 5A; 4.5% MCU/DNA insertion, 25% DNA/MCU backfill, 37% undiluted DNA).

**TABLE 1. X-ray Photoelectron Spectroscopy Atomic Percentages**[a]

| | atomic percentage | |
|---|---|---|
| elements | N 1s | P 2p |
| DNA (predicted) | 18.1 | 4.7 |
| DNA (experimental) | 15.6 ± 0.4 | 3.6 ± 0.1 |
| DNA/MCU Backfill | 13.2 ± 0.3$^{*}$ | 3.1 ± 0.2 |
| MCU/DNA Insertion | 6.9 ± 0.4$^{*,\dagger}$ | 2.0 ± 0.1$^{*,\dagger}$ |
| TEG/DNA Insertion | N/D (1.0)$^{*,\dagger}$ | N/D (0.3)$^{*,\dagger}$ |
| MCU | N/D | N/D |
| TEG | N/D | N/D |

[a] Predicted X-ray photoelectron spectroscopy (XPS) atomic percentages for undiluted DNA were calculated using the numbers of nitrogen and phosphorus atoms in DNA probe molecules. Atomic percentages for undiluted thiolated DNA monolayers (experimental) and mixed monolayers of hydroxyl- (MCU) and tri(ethylene glycol) (TEG)-terminated alkanethiol/DNA on Au substrates were calculated from XPS peak areas ($N$ = 3-6/group). Not detectable XPS signals are indicated by "N/D". Atomic percentages in parentheses are hypothetical lower limits are based on XPS detection limits of 1% and a P/N ratio of 0.3 and are used for statistical purposes. Entries are means ± standard errors of the means. Nitrogen and phosphorus atomic percentages were significantly different across groups ([$F$(3,14) = 280; $P$ < 0.001] and [$F$(3,14) = 135; $P$ < 0.001], respectively). $^{*}P$ < 0.01 *vs* DNA (experimental). $^{\dagger}P$ < 0.001 *vs* DNA/MCU Backfill.

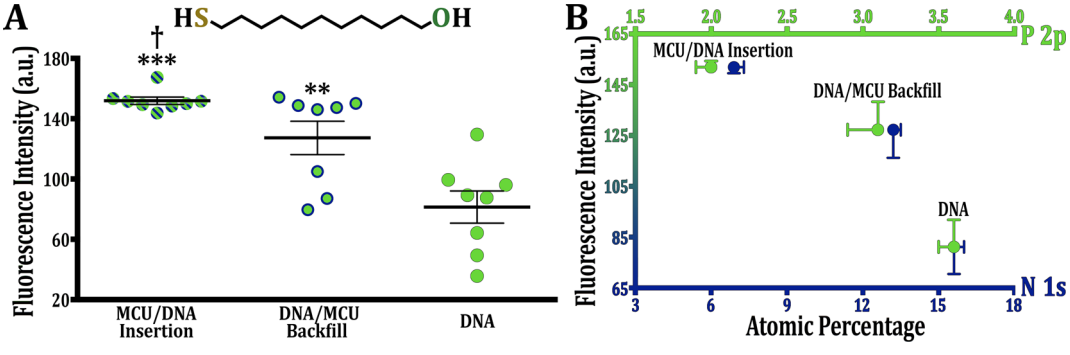


**Figure 5. (A) Fluorescence intensities resulting from hybridization of surface-bound DNA probes and fluorescently labeled complementary DNA target strands on post-lift-off hydroxyl-terminated alkanethiol (MCU) self-assembled monolayers (SAMs) (MCU/DNA Insertion), MCU-backfilled DNA SAMs (DNA/MCU Backfill), and pure DNA SAMs (DNA). Mean fluorescence intensities were significantly different across groups [$F$(2,21) = 16; $P$ < 0.001]. $^{**}P$ < 0.01 and $^{***}P$ < 0.001 *vs* DNA; $^{\dagger}P$ < 0.05 *vs* DNA/MCU Backfill. Error bars represent standard errors of the means with $N$ = 8 substrates per group. (B) Correlations are between fluorescence resulting from DNA hybridization *vs* X-ray photoelectron spectroscopy atomic percentages [N 1s (bottom/blue *x*-axis)/P 2p (top/green *x*-axis)]. Higher fluorescence intensities were correlated with lower DNA probe numbers. Thus, hybridization efficiencies were MCU/DNA Insertion > DNA/MCU Backfill > DNA alone.**

Hybridization efficiencies on Au films and nanoparticles have been determined by various quantification methods including fluorescence-based methods,[7,53,54] electrochemical techniques,[16,49,55,56] "quantitative" XPS,[51] neutron reflectivity measurements,[17] radiometric assays,[57] and surface plasmon resonance spectroscopy.[5,6,21,46] Here, because quantification from fluorescence images and XPS atomic percentages do not provide absolute numbers of DNA probes and targets, we examined relative relationships *via* correlation analysis (Figure 5B) and determined that improved hybridization efficiency is associated with the lift-off lithography-based DNA insertion approach compared to undiluted DNA monolayers and MCU-backfilled DNA SAMs.

**Backfilling Reduces Inserted DNA on Post-Lift-Off Alkanethiol SAMs.** Backfilling with MCU or TEG has been shown to increase target DNA hybridization for Au substrates functionalized first with thiolated probe DNA (Figure 5B).[6,7,21] Here, we investigated the effects of backfilling following lift-off and DNA insertion on MCU and particularly, TEG SAMs. After lift-off and insertion of thiolated DNA probes, we exposed MCU/DNA or TEG/DNA SAMs to additional MCU or TEG molecules, respectively, *via* solution deposition. Backfilling was hypothesized to reduce any remaining DNA–substrate interactions and to increase fluorescence due to greater surface hybridization. On the contrary, we observed *decreases* in the fluorescence intensities of patterns on both post-lift-off MCU (Figure 6A,B) and TEG (Figure 6C,D) SAMs after additional backfilling suggesting that DNA probes were instead removed from substrates.

Removal of DNA probes by backfilling with alkanethiols has been reported.[6,7,21] The purpose of alkanethiol backfilling is to reduce steric interactions between DNA probes and to decrease DNA–substrate interactions. However, when substrates are exposed to alkanethiol backfilling solutions for extended times (>1 h), DNA molecules are displaced and fluorescence decreases due to reduced numbers of surface-bound DNA molecules. Studies by others have shown that DNA probes on MCU-backfilled SAMs diluted by ~50% from pure DNA monolayers required >5 h of backfilling.[7,57] The XPS data above (Table 1, Figure 4A *vs* 4C) indicate ~50% dilution of post-lift-off MCU/DNA *vs* undiluted DNA monolayers. Thus, DNA surface coverages on post-lift-off substrates might be in the regime where additional alkanethiol backfilling removes inserted DNA probes instead of reducing DNA–substrate interactions, which are already presumably minimized. Decreases in fluorescence after backfilling (Figure 6E) suggest that additional incorporation of MCU or TEG molecules reduced the numbers of DNA probe molecules. For TEG, the already low numbers of DNA probes on post-lift-off DNA/SAM-modified substrates were further reduced with additional TEG solution exposure. Therefore, we conclude that alkanethiol backfilling is not advantageous when patterning DNA on Au substrates *via* chemical lift-off lithography.

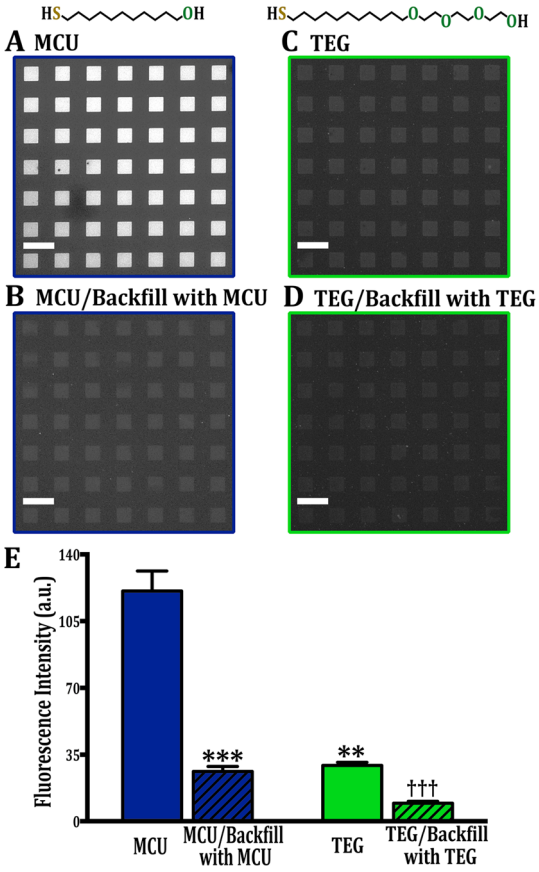


**Figure 6. Representative fluorescence images displaying hybridization of thiolated single-stranded DNA probes with Alexa Fluor 488-labeled target DNA (excitation at 495 nm) on (A,B) hydroxyl-terminated alkanethiol (MCU) or (C,D) tri(ethylene glycol)-terminated alkanethiol (TEG) self-assembled monolayers (SAMs) after lift-off lithography and without or with backfilling with additional respective alkanethiol molecules following probe DNA insertion. After exposing post-lift-off MCU/DNA SAMs to additional MCU, fluorescence was decreased in (B) compared to (A) suggesting that thiolated DNA is displaced by subsequent exposure to additional MCU. Similarly, a weaker fluorescent pattern (D) was observed for backfilled post-lift-off TEG/DNA SAMs compared to the pattern after hybridization on a post-lift-off-alone TEG SAM (C). Fluorescence images (shown with the same exposure times of 5 s) were taken at an emission wavelength of 517 nm. (E) Mean intensities were significantly different for post-lift-off MCU *vs* TEG surfaces without backfilling (A,C) again indicating significant differences with respect to target hybridization (independent replication *vs* Figure 2, two-way ANOVA interaction term [$F(1,4) = 37$, $P < 0.01$]). Error bars represent standard errors of the means with $N = 3$ samples per group. $^{**}P < 0.01$ and $^{***}P < 0.001$ *vs* MCU; $^{\dagger\dagger\dagger}P < 0.001$ *vs* TEG. Scale bars are 50 $\mu$m.**

**DNA Arrays Patterned *via* Lift-Off Lithography Using Longer Functionalized Alkanethiols.** Three terminal ethylene glycol units differentiate TEG from MCU molecules. The additional molecular length of TEG *vs* MCU might reduce DNA access to Au surfaces. Alternately, the presence of the ethylene glycol moieties might have greater

influence on alkanethiol-DNA insertion. To differentiate these possibilities, molecules longer than MCU and TEG, namely mercaptohexadecanol (MCHD) and hexa(ethylene glycol) undecanethiol (HEG) were investigated (Scheme 1). The alkyl backbone of MCHD is five carbon atoms longer than MCU, whereas HEG has the same alkyl backbone as TEG but contains three additional ethylene glycol units.

Previously, we showed by XPS that oxygen plasma treatment of PDMS stamps is needed to lift-off alkanethiols terminated with hydroxyl or amine tail groups.[42] Because interactions at stamp-SAM and SAM-Au interfaces are stronger than Au-Au substrate bonds, post-lift-off PDMS stamps showed Au 4f XPS signals. In contrast, PDMS stamps following conformal contact with relevant SAMs in the absence of oxygen plasma pretreatment did not show Au 4f XPS signals. Here, the chemical lift-off lithography process was carried out on MCHD and HEG SAMs. Post-lift-off PDMS stamps from these SAMs showed Au 4f signals in the XPS spectra (Figure S2A,B) indicating that MCHD and HEG are liftable molecules. While intense fluorescent patterns were observed for MCHD/DNA SAMs (Figure S3A), such patterns were indiscernible for HEG/DNA SAMs (Figure S3B). Thus, although MCHD and HEG molecules are each longer than the corresponding MCU and TEG molecules, respectively, the thicker SAMs formed by MCHD did not hinder DNA probes from accessing Au surfaces. Since the principal differences between MCHD and HEG are the ethylene glycol moieties in the latter, the important finding is that differences in physical lengths between SAM molecules do not by themselves underlie variations in the numbers of tethered DNA probes inserted into post-lift-off regions and associated target DNA hybridization. Instead, ethylene glycol moieties appear to play key roles in limiting the numbers of DNA molecules on post-lift-off oligo(ethylene glycol)-terminated alkanethiol-modified Au surfaces.

**Spectroscopic Evidence for Lift-Off-Induced Conformation Changes in Oligo(Ethylene Glycol) Moieties.** Together, information gleaned from investigating the various hypotheses above suggests that steric hindrance originates from the ethylene glycol moieties of TEG (and HEG). To explore the origin of this effect, polarization-modulation infrared reflection−absorption spectroscopy (PM-IRRAS) was used to monitor the characteristic vibrational feature of ethylene glycol moieties, namely the C−O−C vibrational stretch, before and after chemical lift-off. As for the XPS experiments above, featureless PDMS stamps were used to maximize lift-off areas. For alkanethiols with (ethylene glycol)$_n$ ($n \leq 4$), the C−O−C vibrational band is the dominant IR feature characterizing ethylene glycol moieties.[58]

As shown in Figure 7A, the C−O−C vibrational band displayed a strong, sharp peak at ∼1138 cm$^{-1}$ for pristine TEG SAMs (top curve), indicating a predominantly all-*trans* conformation for the ethylene glycol moieties.[59] However, after lift-off, the C−O−C peak was shifted to ∼1132 cm$^{-1}$ and the peak area was decreased (Figure 7A, bottom curve). Infrared absorption spectra are affected by surface coverage and molecular conformations.[59] While the reduced peak area is likely the result of decreased surface coverage due to the removal of TEG molecules, which is known to occur (*vide supra*), the peak shift is potentially the result of conformational changes in SAM molecules following lift-off. Studies have shown that a C−O−C band at ∼1140 cm$^{-1}$ is attributable to a predominantly all-*trans* conformation, whereas red shifts in the C−O−C stretch indicate transitions to disordered helical conformations.[59,60] The spectroscopic shift from 1138 to 1132 cm$^{-1}$ suggests that TEG molecules undergo rearrangement from ordered nearly all-*trans* to disordered helical conformations following lift-off (Figure 8A), which would reduce DNA probe access to Au surfaces. In contrast, such conformational changes do not occur for MCU SAMs post-lift-off due to the absence of oligo(ethylene glycol) moieties (Figure 8B).

As an additional test that chemical lift-off lithography induces conformational changes in oligo(ethylene glycol) moieties, we investigated tri(ethylene glycol) hexanethiol (TEG-C$_6$) SAMs using infrared spectroscopy before and after lift-off. The TEG-C$_6$ molecules are similar to TEG except their aliphatic backbones consist of 6 *vs* 11 carbons (Scheme 1). As shown in Figure 7B, a C−O−C band was observed at ∼1141 cm$^{-1}$ for pristine TEG-C$_6$ SAMs (top curve). The peak area was reduced after lift-off and shifted to ∼1132 cm$^{-1}$ (bottom curve). Similar to TEG SAMs, these results show that alkanethiols were removed from Au surfaces (smaller peak area). Moreover, the shifted C−O−C band observed with TEG-C$_6$ is characteristic of conformational changes in oligo(ethylene glycol) from pre-lift-off ordered all-*trans* to post-lift-off disordered helical conformations.

For HEG molecules, a broad C−O−C stretch for pre-lift-off SAMs (Figure 7C, top curve) was observed at ∼1127 cm$^{-1}$, which indicates initial predominantly disordered helical conformations for alkanethiols with six or greater ethylene glycol units, in agreement with previous studies.[60,61] After lift-off, the C−O−C peak area decreased due to removal of SAM molecules (Figure 7C, bottom curve). Notably, the C−O−C band did not show a redshift similar to TEG and TEG-C$_6$. This result suggests that HEG SAMs retain the same relative conformation after lift-off. Although HEG molecules did not show conformational changes associated with lift-off lithography, the disordered helical conformation prevented DNA insertion (Figure S3B).

To investigate whether PDMS contact with oligo(ethylene glycol)-terminated SAMs by itself produces disordered ethylene glycol conformations, we monitored the C−O−C stretch arising from methoxy tri(ethylene glycol)-terminated alkanethiol (CH$_3$O-TEG)

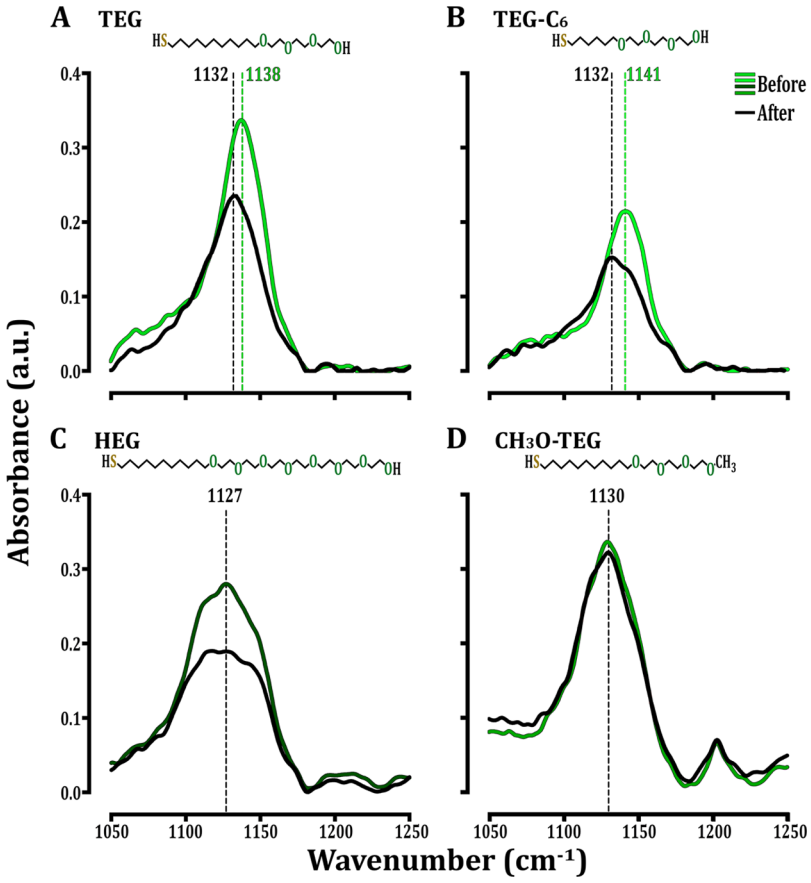


**Figure 7. Representative polarization modulation infrared reflection−absorption spectra of (A) tri(ethylene glycol) undecanethiol (TEG), (B) tri(ethylene glycol) hexanethiol (TEG-$C_6$), (C) hexa(ethylene glycol) undecanethiol (HEG), and (D) methoxy tri(ethylene glycol) undecanethiol ($CH_3O$-TEG) self-assembled monolayers (SAMs) before (top curves) and after (bottom curves) contact with fully oxidized PDMS stamps. Strong C−O−C vibrational bands at ∼1138 $cm^{-1}$ and ∼1141 $cm^{-1}$ are characteristic of ordered all-*trans* tri(ethylene glycol) conformations in (A) TEG and (B) TEG-$C_6$ SAMs prior to lift-off, respectively. (C) A broad C−O−C vibrational band at ∼1127 $cm^{-1}$ is characteristic of disordered helical hexa(ethylene glycol) moieties in HEG SAMs after self-assembly and prior to lift-off. (D) A strong C−O−C vibrational band at ∼1130 $cm^{-1}$ characteristic of amorphous helical tri(ethylene glycol) moieties is also seen with $CH_3O$-TEG SAMs. Peak-area decreases in (A, B, and C) indicate the removal of alkanethiol molecules due to lift-off. (D) Because methoxy groups are not lift-able, the peak area of the C−O−C stretch of $CH_3O$-TEG SAMs remains the same before and after lift-off. The post-lift-off C−O−C bands in (A) and (B) appear shifted from pre-lift-off positions at ∼1138 $cm^{-1}$ and ∼1141 $cm^{-1}$ for TEG and TEG-$C_6$, respectively, to a new position at ∼1132 $cm^{-1}$ indicating conformational changes in tri(ethylene glycol) moieties to disordered helical conformations.**

SAMs with infrared spectroscopy before and after conformal contact with oxygen plasma-treated PDMS stamps. The $CH_3O$-TEG molecules were selected because they are identical to TEG except for the terminal methoxy group (Scheme 1), which prevents subtractive patterning.[42] A sharp C−O−C band was observed at ∼1130 $cm^{-1}$ for pristine $CH_3O$-TEG SAMs, suggestive of initial helical conformations[60] (top curve, Figure 7D). Neither the peak position nor the peak area changed post-lift-off (bottom curve, Figure 7D). The lack of a decrease in peak area indicates that $CH_3O$-TEG molecules were not removed from Au surfaces by contact with activated PDMS stamps. The invariant peak position implies that conformal contact with activated PDMS stamps by itself did not change the conformation of the ethylene glycol moieties. However, the peak position at 1130 $cm^{-1}$ indicates that the $CH_3O$-TEG molecules adopted helical conformations in both pre- and post-lift-off SAMs. Thus, $CH_3O$-TEG SAMs are not ideally suited to testing whether stamp contact alone (*vs* lift-off) underlies the shift from all-*trans* to helical oligo(ethylene glycol) conformations. We have yet to identify oligo(ethylene glycol) alkanethiols best suited for isolating the effects of stamp contact *vs* actual lift-off. These molecules would possess a terminal group not amenable to lift-off yet oligo(ethylene glycol) moieties would adopt an all-*trans* conformation after surface assembly.

The overriding observation from the spectral studies of oligo(ethylene glycol)-terminated alkanethiols is that chemical lift-off lithography induces conformational changes in ethylene glycol segments from ordered to disordered states when the former exist following self-assembly. For TEG and TEG-$C_6$, ordered all-*trans* conformations were converted to disordered helical conformations after lift-off. For HEG, the helical

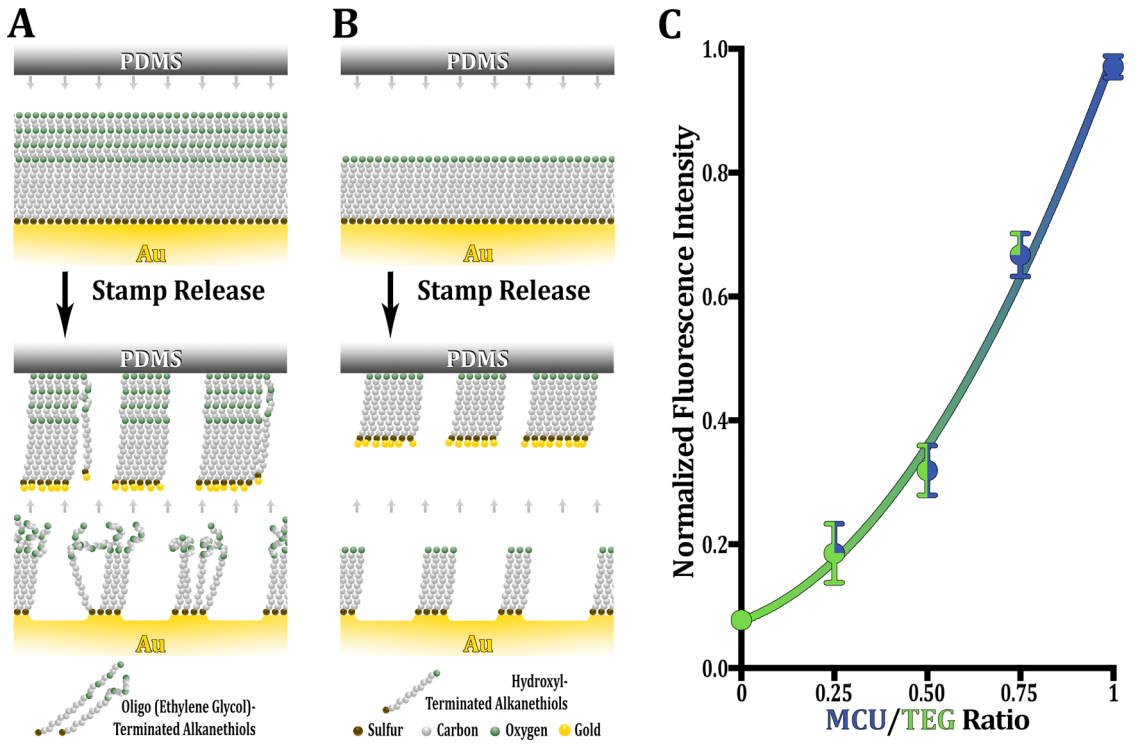


**Figure 8. Schematic (not to scale) illustrating changes in self-assembled monolayers (SAMs) of (A) tri(ethylene glycol)-terminated (TEG) or (B) hydroxyl-terminated (MCU) alkanethiols following conformal contact between oxygen plasma-treated stamps and SAM-modified substrates. The spectroscopic evidence in Figure 7 suggests that ethylene glycol moieties of TEG SAMs undergo conformational changes from ordered all-*trans* conformations prior to chemical lift-off to disordered helical conformations afterward, limiting DNA probe access to Au substrates. In contrast, these conformational changes do not occur for post-lift-off MCU SAMs due to the lack of ethylene glycol moieties. (C) Normalized fluorescence intensities arising from surface hybridization of thiolated DNA probes with fluorescently labeled target DNA *vs* ratios (prior to self-assembly) of MCU molecules in mixed solutions with TEG molecules. The best-fit curve ($R^2 > 0.97$) indicates that by varying the nominal concentration ratios, steric effects resulting from ethylene glycol moieties are controlled to tune surface probe densities and thus, DNA hybridization. Error bars represent standard errors of the mean with $N = 3$ samples per ratio.**

conformation remained the same before and after lift-off. For $CH_3O$-TEG, no conformational or lift-off-related changes occurred. The results of this study as a whole lead to the conclusion that disordered states of oligo(ethylene glycols) existing either prior to lift-off (HEG) or as a result of lift-off (TEG, TEG-$C_6$) are associated with steric hindrance so as to reduce (TEG, TEG-$C_6$) or to prevent (HEG) thiolated DNA insertion into post-lift-off SAMs. Furthermore, greater numbers of ethylene glycol units appear to interfere to a greater extent with DNA insertion following patterning by lift-off lithography. Conversely, increased DNA insertion and/or hybridization can be achieved on TEG SAMs *via* double-lift-off lithography (Figure 2F).

**Mixed MCU/TEG SAMs Modulate DNA Surface Coverage.** Since DNA surface densities are affected differently by MCU *vs* TEG due to the ethylene glycol units in the latter, we examined whether variable combinations of these two types of molecules could be used to advantage to tune DNA access to Au substrates. Mixed composition SAMs have been used to create dilute surface coverages wherein surface tethers are separated and exposed for subsequent chemical modifications, instead of phase segregated.[10,23,39,41,62] As shown in Figure 8C, fluorescence due to surface hybridization between tethered DNA probes and DNA targets increases with respect to solution concentration ratios of MCU *vs* TEG. This relationship indicates that as the fraction of MCU in monolayers increases, steric hindrance from the ethylene glycol moieties in TEG decreases, enabling greater DNA access to the Au surfaces. These results are consistent with the hypothesis that oligo(ethylene glycol) moieties are key factors in regulating DNA surface coverage on post-lift-off SAMs. They further demonstrate that the steric effects resulting from chemical lift-off lithography-induced conformational changes in oligo(ethylene glycol) can be used judiciously to control DNA probe surface coverages.

Fluorescence in Figure 8C resulted from DNA hybridization between surface-bound probes and fluorescently labeled target-DNA. Notably, fluorescence intensities may not directly reflect the actual numbers of surface-bound DNA probes associated with different mixed SAM compositions. Probes already hybridized with target strands may preclude hybridization of additional DNA targets from solution. As such, DNA hybridization may require extended amounts of time (>1 h) to reach saturation at higher probe densities.[63] Also, because we investigated complementary strands with complete base-pair match, some target strands

could have cross-hybridized with two DNA probes at higher probe densities. In such a case, part of a target strand hybridizes with the top segment of one DNA probe and the bottom segment of a neighboring probe. Nonetheless, the data in Figure 8C indicate the dependence and general trends of DNA hybridization on mixed SAM compositions.

Using the MCH backfilling method, Peterson *et al.* reported a DNA surface density of $3 \times 10^{12}$ molecules/cm$^2$ on Au surfaces.[5] Furthermore, Lee *et al.* have reported values of $1.7 \times 10^{13}$ molecules/cm$^2$ and $3.6 \times 10^{13}$ molecules/cm$^2$ for backfilled MCH and oligo(ethylene glycol)-terminated alkanethiols, respectively.[7,21] In contrast, by inserting thiolated DNA into preformed MCH SAMs, Murphy *et al.* and Josephs *et al.* reported low surface densities of $1.1 \times 10^{10}$ molecules/cm$^2$ and $9.5 \times 10^{10}$ molecules/cm$^2$, respectively.[34,35] The extent of insertion depends strongly on the preparation of the matrix into which molecules are placed.[33,38,62] We have previously targeted and reached surface densities between $\sim 2 \times 10^{12}$ molecules/cm$^2$ and $8 \times 10^{13}$ molecules/cm$^2$ *via* insertion.[38,39] In comparison to the backfilling method, correlation analysis of XPS atomic percentages and fluorescence hybridization intensities showed improved hybridization efficiency associated with lower DNA probe surface coverages when using the insertion approach. Thus, we expect that the numbers of DNA probes inserted into post-lift-off MCU or MCHD SAMs are below the upper limit determined for backfilling. Estimations using volume fractions in AFM measurements (shown in Figure 3), with all of the caveats described above, indicate that the tri(ethylene glycol)-terminated (TEG) and hydroxyl-terminated (MCU) SAMs, as prepared and under the conditions described, lead to tethered DNA densities of $3-4 \times 10^{12}$ molecules/cm$^2$ (5−7 pmol/cm$^2$) and $0.8-2 \times 10^{13}$ molecules/cm$^2$ (10−30 pmol/cm$^2$), respectively. These values are consistent with what others and we have observed for insertion of other molecules into SAM matrices.[31,33,64]

## CONCLUSIONS

Subtractive patterning by chemical lift-off lithography relies on strong interactions at stamp-substrate interfaces to remove preassembled alkanethiol SAM molecules from Au substrates. A fundamental advantage of this patterning method is that not all alkanethiol molecules are removed after lift-off within the contacted areas. The remaining molecules create an optimized environment for subsequent insertion and assembly of thiolated DNA probes such that undesirable interactions with substrates are reduced and surface hybridization with target DNA is favored. The extent to which nucleotide surface densities are modulated by post-lift-off SAM molecules depends on specific matrix chemistries and in some cases, the conformations of the terminal SAM moieties.

By creating mixed MCU/TEG SAMs, the surface densities of alkanethiol-DNA probes were tuned according to the nominal concentrations of the two-component SAMs. While post-lift-off TEG SAMs represented the lower limits of tethered DNA surface coverages (with HEG appearing to have negligible DNA inserted), post-lift-off MCU (and to a greater extent MCHD) SAMs represented the upper limits of DNA coverages for the range of SAM molecules investigated here. Expansion of additional parameters such as employing alkanethiols with a wider range of functional groups, altering lengths of ethylene glycol moieties or DNA linkers, and tuning alkanethiol surface coverages and/or packing densities, may enable even greater control of DNA insertion into post-lift-off SAMs. This could broaden the upper and lower limits of DNA surface densities while maintaining highly efficient hybridization.

It is noteworthy that conformational changes in ethylene glycol moieties have been shown to vary with hydration, chain-length, temperature-driven processes, packing densities, surface coverage, and storage conditions.[59,65−67] Our findings show that (ethylene glycol)-terminated alkanethiol conformational changes in SAMs can also be induced by the chemical lift-off process. Moreover, ionic strength, salt concentration, pH, multipoint binding dendrimers, alkyl linkers, and nucleotide-block spacers have been reported to influence thiolated DNA probe coverage.[8,13,63,68] Here, we show that chemical lift-off lithography, in combination with tunable mixed SAM compositions, provides a facile means by which to regulate DNA surface densities.

Probe DNA inserted into native MCH SAM defects has been reported to produce more uniformly distributed DNA monolayers *vs* surface-bound DNA backfilled with MCH.[35] However, it was difficult to achieve high DNA surface densities for practical sensing purposes using insertion alone because of the limited numbers of intrinsic SAM defects. Here, we show that by using lift-off lithography, large-area, high-density DNA patterns can be fabricated by inserting alkanethiol-functionalized DNA probes into post-lift-off alkanethiol SAMs. These findings advance DNA insertion methods toward more practical applications for creating DNA-based sensors. While a single lift-off step removes a large fraction of the preformed SAM molecules, multiple lift-off steps presumably remove additional SAM molecules and/or create additional defects providing greater surface availability for insertion compared to intrinsic SAM/substrate defects.[42] Thus, "artificial defects" introduced into the post-lift-off regions beyond intrinsic defects are key to a highly feasible and advantageous DNA insertion method.

The "artificial defects" created by chemical lift-off lithography appear to comprise a new class of defect site that is serendipitously optimized for insertion and

biorecognition. In the future, molecular-resolution information about the post-lift SAM regions will enable a deeper understanding of their structure. This type of information will also shed light on potential limitations and improve control. The use of scanning probe microscopies to interrogate these SAM structures will be difficult because of their molecular lengths, corrugation, degree of disorder, and association with water molecules under ambient conditions.[69−72] A more precise quantification of the SAM molecules remaining in the stamp-contact regions is feasible using electrochemical reductive desorption, which is sensitive to domain sizes and interaction strengths with different molecules desorbing at different electrochemical potentials.[73−75] Electrochemical reductive desorption measurements will also be useful for determining the numbers and arrangements of alkanethiol molecules remaining on substrates after multiple lift-off steps.

Because lift-off lithography patterning reduces DNA−substrate interactions, when coupled with automated processes for generating arrays, this technique should be applicable for fabricating high-throughput platforms to study aptamer-ligand interactions.[76,77] Notably, the ability to control the surface properties of DNA, the sub-40 nm nanopatterning capabilities of chemical lift-off lithography, and the ability to fabricate high-performance field-effect transistor-based biosensors also *via* lift-off lithography will render single-molecule DNA nanoarrays feasible for bioelectronics and other applications.[78−82]

## METHODS

**Materials.** Silicon substrates coated with 100-nm-thick Au films overlaying 10-nm-thick Ti adhesive layers were purchased from Platypus Technologies (Madison, WI, USA). 11-Mercaptoundecyl tri(ethylene glycol) (TEG) was purchased from Toronto Research Chemicals Inc. (Toronto, ON, Canada). 11-Mercaptoundecanol (MCU) and 0.01 M phosphate buffered saline (PBS) ([NaCl] = 138 mM, [KCl] = 2.7 mM, and [$MgCl_2$] = 5 mM, pH 7.4) were purchased from Sigma-Aldrich (St. Louis, MO, USA). 16-Mercaptohexadecanol (MCHD) was purchased from Dojindo Molecular Technologies (Rockville, MD, USA). 11-Mercaptoundecyl hexa(ethylene glycol) (HEG), (6-mercaptohexyl) tri(ethylene glycol) (TEG-$C_6$), and 11-mercaptoundecyl tri(ethylene glycol) methyl ether ($CH_3O$-TEG) were purchased from ProChimia Surfaces (Sopot, Poland). Absolute ethanol was purchased from Decon Laboratories, Inc. (King of Prussia, PA, USA). Deionized water (~18 MΩ) was obtained from a Millipore water purifier (Billerica, MA, USA). Short single-stranded DNA thiolated at the 5′ end with a hexyl linker (thioMC6-D) (5′-/5-thioMC6-D/GCA CGA AAC CCA AAC CTG ACC TAA CCA ACG TGC T-3′ with molecular weight 10647.2 g/mol and melting temperature 67.2 °C), long thiolated single-stranded DNA (5′-/5ThioMC6-D/TTT TTT TTT TTT TTT TTT TTT TTT TTT TTT TTT GCC GGG CGC GGC GCC GGG GCG CCG TTT TTT TTT TTT TTT TTT TTT TGT GGT TTG GTT GTG TGT G-3′ with molecular weight 31111.2 g/mol and melting temperature 72.0 °C), Alexa 488 fluorophore-conjugated complementary single-stranded DNA molecules (5′-/5-Alex488N/AGC ACG TTG GTT AGG TCA GGT TTG GGT TTC GTG C-3′ with molecular weight 11262.5 g/mol and melting temperature 67.2 °C), and Alexa 488 fluorophore-conjugated noncomplementary, scrambled, single-stranded DNA sequences (5′-/5-Alex488N/CAT GAA CCA ACC CAA GTC AAC GCA AAC GCA TCA A-3′ with molecular weight 11031.4 g/mol and melting temperature 65.3 °C) were purchased from Integrated DNA Technologies (Coralville, IA, USA).[83] All DNA solutions were 100 μM as received and were diluted with 0.01 M PBS pH 7.4 to specific concentrations as needed for each experiment.

**Substrate and Stamp Preparation.** Silicon substrates with Au films were hydrogen-flame annealed. To prepare SAMs, hydroxyl-terminated alkanethiols (MCU, MCHD), hydroxyl tri(ethylene glycol)-terminated alkanethiols (TEG, TEG-$C_6$, HEG), or methoxy tri(ethylene glycol)-terminated alkanethiol ($CH_3O$-TEG) in ethanolic solutions (0.5 mM) were self-assembled on Au substrates for 16−18 h. For controlling DNA surface densities, mixed MCU/TEG SAMs were created by varying the ratios of MCU to TEG in solution concentrations as follows (in mM): 1:0, 0.75:0.25, 0.5:0.5, 0.25:0.75, and 0:1. Following self-assembly, substrates were rinsed thoroughly with ethanol and blown dry with nitrogen gas.

Square (25 μm × 25 μm or 2 μm × 2 μm), protruding features on polydimethylsiloxane (PDMS) stamps were fabricated *via* standard photolithography-processed masters. Details on stamp fabrication and oxygen plasma treatment of PDMS stamps have been published previously.[24,41,42] Briefly, 10:1 mass ratios of SYLGARD 184 silicone elastomer base and curing agent (Ellsworth Adhesives, Germantown, WI, USA) were mixed thoroughly in a plastic cup, degassed under a vacuum, cast onto master substrates in a plastic Petri dish, and then cured in an oven at 70 °C overnight. The polymerized stamps were removed from the masters, cut into appropriate sizes, rinsed with ethanol, and blown dry with nitrogen gas. Stamps were then exposed to oxygen plasma (Harrick Plasma, power 18 W, and oxygen pressure 10 psi) for 30 s, yielding hydrophilic, reactive PDMS surfaces.[42] After lift-off, PDMS stamps were rinsed with ethanol, wiped with Kimberly-Clark tissues soaked in ethanol, and dried with nitrogen gas. Cleaned stamps were sealed to clean glass slides for storage before additional use.

**Patterning Alkanethiol Self-Assembled Monolayer (SAM)-Modified Substrates *via* Chemical Lift-Off Lithography.** Oxygen plasma-treated PDMS stamps were brought into conformal contact with SAM-modified substrates for ~6 h for single lift-off. The contact reactions at the stamp-SAM interfaces caused SAM molecules to be removed specifically in the contact regions once the PDMS stamps were released from the substrates. After patterning, substrates were rinsed with ethanol and dried with nitrogen gas.

Double lift-off on TEG SAMs involved a combination of flat (featureless) and patterned PDMS stamps. The first lift-off step was carried out using flat stamps for 3 h to remove molecules from the entire surface. In the second lift-off step, patterned stamps were sealed to the post-lift-off substrates for another 3 h to remove molecules only in the contact regions between the stamp features and the surfaces. The shorter stamp/substrate contact times (3 h *vs* 6 h) were selected to expedite DNA pattern generation. We previously found that patterns were created *via* CLL at even shorter times (*i.e.*, 1 and 5 min).[42,82] Thus, exploring short stamp/substrate contact times (<3 h) may be beneficial for practical applications associated with generating CLL-based DNA arrays.

For fluorescence experiments, substrates were incubated in solutions of 1 μM DNA probes in 0.01 M PBS pH 7.4 for ~17 h to insert DNA into the post-lift-off exposed Au areas.[8] After incubation, substrates were rinsed thoroughly with deionized water and blown to dryness with nitrogen gas. To visualize DNA hybridization, substrates were exposed to solutions of 1 μM target DNA in 0.01 M PBS pH 7.4 for ~1 h. Substrates were processed in pairs for MCU and TEG SAMs. One substrate was incubated with target DNA and the other with noncomplementary DNA as a control. Each experiment was repeated at least three times over a minimum of three different days. Variations in fluorescence intensities across experiments can arise due to the sensitivity of DNA hybridization to $Mg^{2+}$ concentrations in incubation buffers.[68] However, this factor should affect all

substrates processed in parallel equally within each experiment. Thus, it is important to process samples in parallel as much as possible and to include appropriate control samples (*e.g.*, hybridization to noncomplementary DNA) in all sample runs.

Deionized water was used to rinse the substrates gently before imaging under an inverted fluorescence microscope (Axio Observer.D1, Carl Zeiss MicroImaging, Inc., Thornwood, NY, USA) using a fluorescence filter set (38 HE/high efficiency) having excitation and emission wavelengths of 470 ± 20 nm and 525 ± 25 nm, respectively. Fluorescence intensity was measured with the line profile function in AxioVs40 V 4.7.1.0 software (Carl Zeiss MicroImaging, Inc., Thornwood, USA). The widths of the fluorescence line scans were made to be approximately the same as that of the square patterned features (*i.e.*, 25 $\mu$m). On average, three to four fluorescence line scans were acquired per image. Fluorescence intensity was averaged for each line scan and then for each image. Alternately, for substrates without patterns, fluorescence intensity was measured using a histogram function and similarly defined areas across all fluorescence images. In all cases, three fluorescence measurements were made per substrate. Specific fluorescence intensities measured on post-lift-off substrates are the differences between the DNA hybridization regions (square features) and the alkanethiol backgrounds (absence of DNA probes).

Backfilling experiments following CLL were performed using the same procedures as those described above with the exception that after DNA probe incubation, substrates were further incubated with 0.5 mM MCU diluted with 0.01 M PBS pH 7.4 to make 10 $\mu$M MCU solutions for backfilling MCU/DNA SAMs for 30 min.[7] Similarly, solutions of 0.5 mM TEG were diluted with 0.01 M PBS pH 7.4 to make 50 $\mu$M TEG solutions for backfilling after CLL.[21] The traditional backfilling method was carried out by incubating hydrogen-flame annealed Au substrates with 1 $\mu$M DNA-probe solutions for ~17 h followed by backfilling with 10 $\mu$M MCU solution for 30 min. Dilution with PBS was used to minimize the deleterious effect that ethanol can have on DNA probes assembled on surfaces.[28]

For atomic force microscopy (AFM) and X-ray photoelectron spectroscopy (XPS) experiments, post-lift-off substrates were incubated with solutions of 1 $\mu$M long (100 base) or short (34 base) DNA probes in 0.01 M PBS pH 7.4 for ~17 h, rinsed gently with deionized water and blown dry with nitrogen gas.[8] Tapping mode AFM (Dimension 5000, Bruker AXS, Santa Barbara, CA, USA) was used to characterize height differences on DNA/alkanethiol mixed monolayers on the post-lift-off substrates. Topographic AFM images were collected using Si cantilevers with a spring constant of 48 N/m and a resonant frequency of 190 kHz (Veeco Instruments, Santa Barbara, CA, USA).

For XPS experiments, featureless PDMS stamps were used for the chemical lift-off process. All XPS data were collected using an AXIS Ultra DLD instrument (Kratos Analytical Inc., Chestnut Ridge, NY, USA). A monochromatic Al K$\alpha$ X-ray source (10 mA for survey scans and 20 mA for high resolution scans, 15 kV) with a 200 $\mu$m circular spot size and ultrahigh vacuum ($10^{-9}$ Torr) were used.[41,42] Spectra were acquired at a pass energy of 160 eV for survey spectra and 20 eV for high resolution spectra of C 1s, O 1s, N 1s, P 2p, S 2p, and Au 4f regions using a 200 ms dwell time. Different numbers of scans were carried out depending on the difficulty of identifying each peak *vs* background, ranging from 20 scans for C 1s to 100 for Au 4f. All XPS peaks for each element on Au substrates were referenced to the Au 4f signal at 84.0 eV. Atomic percentages were calculated from peak areas.

Because PDMS is an insulator, a charge neutralizer (flood gun) was used to obtain signals from each element on PDMS stamps. As a result, peaks are shifted slightly from their expected regions (for C 1s this is 4−5 eV lower than the reference at 284.0 eV). Because the number of peaks of interest was small (only Au 4f peaks on PDMS samples), and they were well separated (~4 eV), peak shifting did not affect identification. No corrections were carried out during data collection to shift peaks back to particular regions or to scale peaks based on reference locations.

Featureless PDMS stamps were also used for the chemical lift-off process for infrared spectroscopy experiments. Polarization modulation infrared reflection−absorption spectroscopy (PM-IRRAS) was carried out using a Thermo Nicolet 8700 Fourier-transform infrared spectrometer (Thermo Electron Corp., Madison, WI, USA) in reflectance mode using infrared light incident at 80° relative to the surface normal. Spectra with 1024 scans and a resolution of 4 $cm^{-1}$ were collected in all cases. Each PM-IRRAS experiment was carried out at least four times. Polarization modulation infrared reflection−absorption spectroscopy was used to investigate the removal of molecules due to lift-off by monitoring the peak areas of the O−H stretching band associated with hydroxyl terminal groups. This spectroscopic method was also used to detect the conformational changes of oligo(ethylene glycols) in TEG, TEG-$C_6$, HEG, and $CH_3O$-TEG alkanethiols.

**Statistical Analyses.** Data from fluorescence microscopy, XPS atomic percentage, and AFM topography experiments were initially analyzed by one-way or two-way analysis of variance as appropriate, followed by Tukey's multiple group comparisons. *A priori* individual group comparisons for fluorescence microscopy data were also analyzed by two-tailed unpaired Student's *t*-tests. All statistics were carried out using GraphPad Prism (GraphPad Software Inc., San Diego, USA). Data are reported as means ± standard errors of the means with probabilities of $P < 0.05$ considered statistically significant.

*Conflict of Interest:* The authors declare no competing financial interest.

*Supporting Information Available:* The Supporting Information is available free of charge on the ACS Publications website at DOI: 10.1021/acsnano.5b05546.

Experimental procedures and supplemental experiments. (PDF)

*Acknowledgment.* This work was supported by the U.S. Department of Energy (#DE-SC0005025) for the patterning and measurements, the Cal-BRAIN Neurotechnology Program, and the UCLA Weil Endowment Fund for Research. The authors would like to thank Mr. Jeffrey Schwartz, Prof. Scott Day, Dr. Andre Nel, Dr. Ignacio Martini, the Materials Laboratory at the Molecular Instrumentation Center, and the California NanoSystems Institute Nano and Pico Characterization Facility for assistance with experiments and manuscript preparation. The experiments were designed by all authors and carried out by HHC, NN, WSL, SC, and ACS. Data were analyzed by HHC, ACS, HY, PSW, and AMA. Figures were prepared by HY and HHC. The manuscript was written by HHC, PSW, and AMA with assistance from NN, ACS, WSL, SC, and HY.

## REFERENCES AND NOTES

1. Lockhart, D. J.; Winzeler, E. A. Genomics, Gene Expression and DNA Arrays. *Nature* **2000**, *405*, 827–836.
2. Caruso, F.; Rodda, E.; Furlong, D. N.; Haring, V. DNA Binding and Hybridization on Gold and Derivatized Surfaces. *Sens. Actuators, B* **1997**, *41*, 189–197.
3. Sassolas, A.; Leca-Bouvier, B. D.; Blum, L. J. DNA Biosensors and Microarrays. *Chem. Rev.* **2008**, *108*, 109–139.
4. Herne, T. M.; Tarlov, M. J. Characterization of DNA Probes Immobilized on Gold Surfaces. *J. Am. Chem. Soc.* **1997**, *119*, 8916–8920.
5. Peterson, A. W.; Heaton, R. J.; Georgiadis, R. M. The Effect of Surface Probe Density on DNA Hybridization. *Nucleic Acids Res.* **2001**, *29*, 5163–5168.
6. Boozer, C.; Chen, S. F.; Jiang, S. Y. Controlling DNA Orientation on Mixed ssDNA/OEG SAMs. *Langmuir* **2006**, *22*, 4694–4698.
7. Lee, C.-Y.; Gong, P.; Harbers, G. M.; Grainger, D. W.; Castner, D. G.; Gamble, L. J. Surface Coverage and Structure of Mixed DNA/Alkylthiol Monolayers on Gold: Characterization by XPS, NEXAFS, and Fluorescence Intensity Measurements. *Anal. Chem.* **2006**, *78*, 3316–3325.
8. Day, B. S.; Fiegland, L. R.; Vint, E. S.; Shen, W.; Morris, J. R.; Norton, M. L. Thiolated Dendrimers as Multi-Point Binding Headgroups for DNA Immobilization on Gold. *Langmuir* **2011**, *27*, 12434–12442.

9. Ostuni, E.; Yan, L.; Whitesides, G. M. The Interaction of Proteins and Cells with Self-Assembled Monolayers of Alkanethiolates on Gold and Silver. *Colloids Surf., B* **1999**, *15*, 3–30.
10. Shuster, M. J.; Vaish, A.; Cao, H. H.; Guttentag, A. I.; McManigle, J. E.; Gibb, A. L.; Martinez, M. M.; Nezarati, R. M.; Hinds, J. M.; Liao, W.-S.; Weiss, P. S.; Andrews, A. M. Patterning Small-Molecule Biocapture Surfaces: Microcontact Insertion Printing *vs*. Photolithography. *Chem. Commun.* **2011**, *47*, 10641–10643.
11. Huang, E.; Zhou, F. M.; Deng, L. Studies of Surface Coverage and Orientation of DNA Molecules Immobilized onto Preformed Alkanethiol Self-Assembled Monolayers. *Langmuir* **2000**, *16*, 3272–3280.
12. Rant, U.; Arinaga, K.; Fujita, S.; Yokoyama, N.; Abstreiter, G.; Tornow, M. Structural Properties of Oligonucleotide Monolayers on Gold Surfaces Probed by Fluorescence Investigations. *Langmuir* **2004**, *20*, 10086–10092.
13. Opdahl, A.; Petrovykh, D. Y.; Kimura-Suda, H.; Tarlov, M. J.; Whitman, L. J. Independent Control of Grafting Density and Conformation of Single-Stranded DNA Brushes. *Proc. Natl. Acad. Sci. U. S. A.* **2007**, *104*, 9–14.
14. Kaufmann, R.; Averbukh, I.; Naaman, R.; Daube, S. S. Controlling the Reactivity of Adsorbed DNA on Template Surfaces. *Langmuir* **2008**, *24*, 927–931.
15. Howell, C.; Zhao, J. L.; Koelsch, P.; Zharnikov, M. Hybridization in ssDNA Films-A Multi-Technique Spectroscopy Study. *Phys. Chem. Chem. Phys.* **2011**, *13*, 15512–15522.
16. Steel, A. B.; Herne, T. M.; Tarlov, M. J. Electrochemical Quantitation of DNA Immobilized on Gold. *Anal. Chem.* **1998**, *70*, 4670–4677.
17. Levicky, R.; Herne, T. M.; Tarlov, M. J.; Satija, S. K. Using Self-Assembly to Control the Structure of DNA Monolayers on Gold: A Neutron Reflectivity Study. *J. Am. Chem. Soc.* **1998**, *120*, 9787–9792.
18. Kimura-Suda, H.; Petrovykh, D. Y.; Tarlov, M. J.; Whitman, L. J. Base-Dependent Competitive Adsorption of Single-Stranded DNA on Gold. *J. Am. Chem. Soc.* **2003**, *125*, 9014–9015.
19. Arinaga, K.; Rant, U.; Tornow, M.; Fujita, S.; Abstreiter, G.; Yokoyama, N. The Role of Surface Charging During the Coadsorption of Mercaptohexanol to DNA Layers on Gold: Direct Observation of Desorption and Layer Reorientation. *Langmuir* **2006**, *22*, 5560–5562.
20. Lai, R. Y.; Seferos, D. S.; Heeger, A. J.; Bazan, G. C.; Plaxco, K. W. Comparison of the Signaling and Stability of Electrochemical DNA Sensors Fabricated from 6- or 11-Carbon Self-Assembled Monolayers. *Langmuir* **2006**, *22*, 10796–10800.
21. Lee, C.-Y.; Gamble, L. J.; Grainger, D. W.; Castner, D. G. Mixed DNA/Oligo (Ethylene Glycol) Functionalized Gold Surfaces Improve DNA Hybridization in Complex Media. *Biointerphases* **2006**, *1*, 82–92.
22. Boozer, C.; Ladd, J.; Chen, S. F.; Yu, Q.; Homola, J.; Jiang, S. Y. DNA Directed Protein Immobilization on Mixed ssDNA/Oligo(Ethylene Glycol) Self-Assembled Monolayers for Sensitive Biosensors. *Anal. Chem.* **2004**, *76*, 6967–6972.
23. Shuster, M. J.; Vaish, A.; Szapacs, M. E.; Anderson, M. E.; Weiss, P. S.; Andrews, A. M. Biospecific Recognition of Tethered Small Molecules Diluted in Self-Assembled Monolayers. *Adv. Mater.* **2008**, *20*, 164–167.
24. Liao, W.-S.; Cao, H. H.; Cheunkar, S.; Shuster, M. J.; Altieri, S. C.; Weiss, P. S.; Andrews, A. M. Small-Molecule Arrays for Sorting G-Protein-Coupled Receptors. *J. Phys. Chem. C* **2013**, *117*, 22362–22368.
25. Choi, S.; Murphy, W. L. Multifunctional Mixed SAMs That Promote Both Cell Adhesion and Noncovalent DNA Immobilization. *Langmuir* **2008**, *24*, 6873–6880.
26. Satjapipat, M.; Sanedrin, R.; Zhou, F. M. Selective Desorption of Alkanethiols in Mixed Self-Assembled Monolayers for Subsequent Oligonucleotide Attachment and DNA Hybridization. *Langmuir* **2001**, *17*, 7637–7644.
27. Aqua, T.; Naaman, R.; Daube, S. S. Controlling the Adsorption and Reactivity of DNA on Gold. *Langmuir* **2003**, *19*, 10573–10580.
28. Fang, Y.; Spisz, T. S.; Hoh, J. H. Ethanol-Induced Structural Transitions of DNA on Mica. *Nucleic Acids Res.* **1999**, *27*, 1943–1949.
29. Kick, A.; Boensch, M.; Kummer, K.; Vyalikh, D. V.; Molodtsov, S. L.; Mertig, M. Controlling Structural Properties of Self-Assembled Oligonucleotide-Mercaptohexanol Monolayers. *J. Electron Spectrosc. Relat. Phenom.* **2009**, *172*, 36–41.
30. Bumm, L. A.; Arnold, J. J.; Cygan, M. T.; Dunbar, T. D.; Burgin, T. P.; Jones, L.; Allara, D. L.; Tour, J. M.; Weiss, P. S. Are Single Molecular Wires Conducting? *Science* **1996**, *271*, 1705–1707.
31. Cygan, M. T.; Dunbar, T. D.; Arnold, J. J.; Bumm, L. A.; Shedlock, N. F.; Burgin, T. P.; Jones, L.; Allara, D. L.; Tour, J. M.; Weiss, P. S. Insertion, Conductivity, and Structures of Conjugated Organic Oligomers in Self-Assembled Alkanethiol Monolayers on Au{111}. *J. Am. Chem. Soc.* **1998**, *120*, 2721–2732.
32. Shuster, M. J.; Vaish, A.; Gilbert, M. L.; Martinez-Rivera, M.; Nezarati, R. M.; Weiss, P. S.; Andrews, A. M. Comparison of Oligo(Ethylene Glycol)Alkanethiols *versus n*-Alkanethiols: Self-Assembly, Insertion, and Functionalization. *J. Phys. Chem. C* **2011**, *115*, 24778–24787.
33. Claridge, S. A.; Liao, W.-S.; Thomas, J. C.; Zhao, Y.; Cao, H. H.; Cheunkar, S.; Serino, A. C.; Andrews, A. M.; Weiss, P. S. From the Bottom Up: Dimensional Control and Characterization in Molecular Monolayers. *Chem. Soc. Rev.* **2013**, *42*, 2725–2745.
34. Murphy, J. N.; Cheng, A. K. H.; Yu, H.-Z.; Bizzotto, D. On the Nature of DNA Self-Assembled Monolayers on Au: Measuring Surface Heterogeneity with Electrochemical in Situ Fluorescence Microscopy. *J. Am. Chem. Soc.* **2009**, *131*, 4042–4050.
35. Josephs, E. A.; Ye, T. Nanoscale Spatial Distribution of Thiolated DNA on Model Nucleic Acid Sensor Surfaces. *ACS Nano* **2013**, *7*, 3653–3660.
36. Josephs, E. A.; Ye, T. A Single-Molecule View of Conformational Switching of DNA Tethered to a Gold Electrode. *J. Am. Chem. Soc.* **2012**, *134*, 10021–10030.
37. Josephs, E. A.; Ye, T. Electric-Field Dependent Conformations of Single DNA Molecules on a Model Biosensor Surface. *Nano Lett.* **2012**, *12*, 5255–5261.
38. Mullen, T. J.; Srinivasan, C.; Hohman, J. N.; Gillmor, S. D.; Shuster, M. J.; Horn, M. W.; Andrews, A. M.; Weiss, P. S. Microcontact Insertion Printing. *Appl. Phys. Lett.* **2007**, *90*, 0631141–0631143.
39. Vaish, A.; Shuster, M. J.; Cheunkar, S.; Singh, Y. S.; Weiss, P. S.; Andrews, A. M. Native Serotonin Membrane Receptors Recognize 5-Hydroxytryptophan-Functionalized Substrates: Enabling Small-Molecule Recognition. *ACS Chem. Neurosci.* **2010**, *1*, 495–504.
40. Saavedra, H. M.; Mullen, T. J.; Zhang, P. P.; Dewey, D. C.; Claridge, S. A.; Weiss, P. S. Hybrid Strategies in Nanolithography. *Rep. Prog. Phys.* **2010**, *73*, 0365011–03650140.
41. Vaish, A.; Shuster, M. J.; Cheunkar, S.; Weiss, P. S.; Andrews, A. M. Tuning Stamp Surface Energy for Soft Lithography of Polar Molecules to Fabricate Bioactive Small-Molecule Microarrays. *Small* **2011**, *7*, 1471–1479.
42. Liao, W.-S.; Cheunkar, S.; Cao, H. H.; Bednar, H. R.; Weiss, P. S.; Andrews, A. M. Subtractive Patterning *via* Chemical Lift-Off Lithography. *Science* **2012**, *337*, 1517–1521.
43. Kung, L. A.; Kam, L.; Hovis, J. S.; Boxer, S. G. Patterning Hybrid Surfaces of Proteins and Supported Lipid Bilayers. *Langmuir* **2000**, *16*, 6773–6776.
44. Hovis, J. S.; Boxer, S. G. Patterning Barriers to Lateral Diffusion in Supported Lipid Bilayer Membranes by Blotting and Stamping. *Langmuir* **2000**, *16*, 894–897.
45. Hovis, J. S.; Boxer, S. G. Patterning and Composition Arrays of Supported Lipid Bilayers by Microcontact Printing. *Langmuir* **2001**, *17*, 3400–3405.
46. Peterson, A. W.; Heaton, R. J.; Georgiadis, R. Kinetic Control of Hybridization in Surface Immobilized DNA Monolayer Films. *J. Am. Chem. Soc.* **2000**, *122*, 7837–7838.
47. Rao, A. N.; Grainger, D. W. Biophysical Properties of Nucleic Acids at Surfaces Relevant to Microarray Performance. *Biomater. Sci.* **2014**, *2*, 436–471.

48. Damaschun, G.; Damaschun, H.; Misselwitz, R.; Pospelov, V. A.; Zalenskaya, I. A.; Zirwer, D.; Muller, J. J.; Vorobev, V. I. How Many Base-Pairs per Turn Does DNA Have in Solution and in Chromatin - an Answer from Wide-Angle X-Ray-Scattering. *Biomed. Biochim. Acta* **1983**, *42*, 697–703.
49. Steel, A. B.; Levicky, R. L.; Herne, T. M.; Tarlov, M. J. Immobilization of Nucleic Acids at Solid Surfaces: Effect of Oligonucleotide Length on Layer Assembly. *Biophys. J.* **2000**, *79*, 975–981.
50. May, C. J.; Canavan, H. E.; Castner, D. G. Quantitative X-Ray Photoelectron Spectroscopy and Time-Of-Flight Secondary Ion Mass Spectrometry Characterization of the Components in DNA. *Anal. Chem.* **2004**, *76*, 1114–1122.
51. Petrovykh, D. Y.; Kimura-Suda, H.; Tarlov, M. J.; Whitman, L. J. Quantitative Characterization of DNA Films by X-Ray Photoelectron Spectroscopy. *Langmuir* **2004**, *20*, 429–440.
52. Lee, C. Y.; Nguyen, P. C. T.; Grainger, D. W.; Gamble, L. J.; Castner, D. G. Structure and DNA Hybridization Properties of Mixed Nucleic Acid/Maleimide-Ethylene Glycol Monolayers. *Anal. Chem.* **2007**, *79*, 4390–4400.
53. Cederquist, K. B.; Keating, C. D. Hybridization Efficiency of Molecular Beacons Bound to Gold Nanowires: Effect of Surface Coverage and Target Length. *Langmuir* **2010**, *26*, 18273–18280.
54. Demers, L. M.; Mirkin, C. A.; Mucic, R. C.; Reynolds, R. A.; Letsinger, R. L.; Elghanian, R.; Viswanadham, G. A Fluorescence-Based Method for Determining the Surface Coverage and Hybridization Efficiency of Thiol-Capped Oligonucleotides Bound to Gold Thin Films and Nanoparticles. *Anal. Chem.* **2000**, *72*, 5535–5541.
55. Gorodetsky, A. A.; Buzzeo, M. C.; Barton, J. K. DNA-Mediated Electrochemistry. *Bioconjugate Chem.* **2008**, *19*, 2285–2296.
56. Kelley, S. O.; Jackson, N. M.; Hill, M. G.; Barton, J. K. Long-Range Electron Transfer through DNA Films. *Angew. Chem., Int. Ed.* **1999**, *38*, 941–945.
57. Gong, P.; Lee, C. Y.; Gamble, L. J.; Castner, D. G.; Grainger, D. W. Hybridization Behavior of Mixed DNA/Alkylthiol Monolayers on Gold: Characterization by Surface Plasmon Resonance and P-32 Radiometric Assay. *Anal. Chem.* **2006**, *78*, 3326–3334.
58. Valiokas, R.; Malysheva, L.; Onipko, A.; Lee, H.-H.; Ruzele, Z.; Svedhem, S.; Svensson, S. C. T.; Gelius, U.; Liedberg, B. On the Quality and Structural Characteristics of Oligo-(Ethylene Glycol) Assemblies on Gold: An Experimental and Theoretical Study. *J. Electron Spectrosc. Relat. Phenom.* **2009**, *172*, 9–20.
59. Skoda, M. W. A.; Jacobs, R. M. J.; Willis, J.; Schreiber, F. Hydration of Oligo(Ethylene Glycol) Self-Assembled Monolayers Studied Using Polarization Modulation Infrared Spectroscopy. *Langmuir* **2007**, *23*, 970–974.
60. Harder, P.; Grunze, M.; Dahint, R.; Whitesides, G. M.; Laibinis, P. E. Molecular Conformation in Oligo(Ethylene Glycol)-Terminated Self-Assembled Monolayers on Gold and Silver Surfaces Determines Their Ability to Resist Protein Adsorption. *J. Phys. Chem. B* **1998**, *102*, 426–436.
61. Zorn, S.; Martin, N.; Gerlach, A.; Schreiber, F. Real-Time PMIRRAS Studies of *in Situ* Growth of $C_{11}Eg_6OMe$ on Gold and Immersion Effects. *Phys. Chem. Chem. Phys.* **2010**, *12*, 8986–8991.
62. Weck, M.; Jackiw, J. J.; Rossi, R. R.; Weiss, P. S.; Grubbs, R. H. Ring-Opening Metathesis Polymerization from Surfaces. *J. Am. Chem. Soc.* **1999**, *121*, 4088–4089.
63. Wong, E. L. S.; Chow, E.; Gooding, J. J. DNA Recognition Interfaces: The Influence of Interfacial Design on the Efficiency and Kinetics of Hybridization. *Langmuir* **2005**, *21*, 6957–6965.
64. Smith, R. K.; Nanayakkara, S. U.; Woehrle, G. H.; Pearl, T. P.; Blake, M. M.; Hutchison, J. E.; Weiss, P. S. Spectral Diffusion in the Tunneling Spectra of Ligand-Stabilized Undecagold Clusters. *J. Am. Chem. Soc.* **2006**, *128*, 9266–9267.
65. Valiokas, R.; Svedhem, S.; Ostblom, M.; Svensson, S. C. T.; Liedberg, B. Influence of Specific Intermolecular Interactions on the Self-Assembly and Phase Behavior of Oligo-(Ethylene Glycol)-Terminated Alkanethiolates on Gold. *J. Phys. Chem. B* **2001**, *105*, 5459–5469.
66. Zorn, S.; Skoda, M. W. A.; Gerlach, A.; Jacobs, R. M. J.; Schreiber, F. On the Stability of Oligo(Ethylene Glycol) ($C_{11}EG_6OMe$) SAMs on Gold: Behavior at Elevated Temperature in Contact with Water. *Langmuir* **2011**, *27*, 2237–2243.
67. Zorn, S.; Dettinger, U.; Skoda, M. W. A.; Jacobs, R. M. J.; Peisert, H.; Gerlach, A.; Chasse, T.; Schreiber, F. Stability of Hexa(Ethylene Glycol) SAMs towards the Exposure to Natural Light and Repeated Reimmersion. *Appl. Surf. Sci.* **2012**, *258*, 7882–7888.
68. Ravan, H.; Kashanian, S.; Sanadgol, N.; Badoei-Dalfard, A.; Karami, Z. Strategies for Optimizing DNA Hybridization on Surfaces. *Anal. Biochem.* **2014**, *444*, 41–46.
69. Esplandiu, M. J.; Hagenstrom, H.; Kolb, D. M. Functionalized Self-Assembled Alkanethiol Monolayers on Au(111) Electrodes: 1. Surface Structure and Electrochemistry. *Langmuir* **2001**, *17*, 828–838.
70. Liu, Y. F.; Yang, Y. C.; Lee, Y. L. Assembly Behavior and Monolayer Characteristics of OH-Terminated Alkanethiol on Au(111): *In Situ* Scanning Tunneling Microscopy and Electrochemical Studies. *Nanotechnology* **2008**, *19*, 065609.
71. Liu, Y. F.; Lee, Y. L. Adsorption Characteristics of OH-Terminated Alkanethiol and Arenethiol on Au(111) Surfaces. *Nanoscale* **2012**, *4*, 2093–2100.
72. Abel, G. R.; Josephs, E. A.; Luong, N.; Ye, T. A Switchable Surface Enables Visualization of Single DNA Hybridization Events with Atomic Force Microscopy. *J. Am. Chem. Soc.* **2013**, *135*, 6399–6402.
73. Mullen, T. J.; Dameron, A. A.; Weiss, P. S. Directed Assembly and Separation of Self-Assembled Monolayers *via* Electrochemical Processing. *J. Phys. Chem. B* **2006**, *110*, 14410–14417.
74. Dameron, A. A.; Mullen, T. J.; Hengstebeck, R. W.; Saavedra, H. M.; Weiss, P. S. Origins of Displacement in 1-Adamantanethiolate Self-Assembled Monolayers. *J. Phys. Chem. C* **2007**, *111*, 6747–6752.
75. Kim, M.; Hohman, J. N.; Serino, A. C.; Weiss, P. S. Structural Manipulation of Hydrogen-Bonding Networks in Amide-Containing Alkanethiolate Monolayers *via* Electrochemical Processing. *J. Phys. Chem. C* **2010**, *114*, 19744–19751.
76. Gao, P.; Cai, Y. G. Aptamer Fiber Anchored on the Edge of a Protein Pattern: A Template for Nanowire Fabrication. *ACS Nano* **2009**, *3*, 3475–3484.
77. Sheng, W. A.; Chen, T.; Tan, W. H.; Fan, Z. H. Multivalent DNA Nanospheres for Enhanced Capture of Cancer Cells in Microfluidic Devices. *ACS Nano* **2013**, *7*, 7067–7076.
78. Wilson, N. A.; Abu-Shumays, R.; Gyarfas, B.; Wang, H.; Lieberman, K. R.; Akeson, M.; Dunbar, W. B. Electronic Control of DNA Polymerase Binding and Unbinding to Single DNA Molecules. *ACS Nano* **2009**, *3*, 995–1003.
79. Yasui, T.; Rahong, S.; Motoyama, K.; Yanagida, T.; Wu, Q.; Kaji, N.; Kanai, M.; Doi, K.; Nagashima, K.; Tokeshi, M.; Taniguchi, M.; Kawano, S.; Kawai, T.; Baba, Y. DNA Manipulation and Separation in Sublithographic-Scale Nanowire Array. *ACS Nano* **2013**, *7*, 3029–3035.
80. Fu, Y. M.; Zeng, D. D.; Chao, J.; Jin, Y. Q.; Zhang, Z.; Liu, H. J.; Li, D.; Ma, H. W.; Huang, Q.; Gothelf, K. V.; Fan, C. H. Single-Step Rapid Assembly of DNA Origami Nanostructures for Addressable Nanoscale Bioreactors. *J. Am. Chem. Soc.* **2013**, *135*, 696–702.
81. Liao, W. S.; Chen, X.; Yang, T. L.; Castellana, E. T.; Chen, J. X.; Cremer, P. S. Benchtop Chemistry for the Rapid Prototyping of Label-Free Biosensors: Transmission Localized Surface Plasmon Resonance Platforms. *Biointerphases* **2009**, *4*, 80–85.
82. Kim, J.; Rim, Y. S.; Chen, H. J.; Cao, H. H.; Nakatsuka, N.; Hinton, H. L.; Zhao, C. Z.; Andrews, A. M.; Yang, Y.; Weiss, P. S. Fabrication of High-Performance Ultrathin $In_2O_3$ Film Field-Effect Transistors and Biosensors Using Chemical Lift-Off Lithography. *ACS Nano* **2015**, *9*, 4572–4582.
83. Yang, X. J.; Bing, T.; Mei, H. C.; Fang, C. L.; Cao, Z. H.; Shangguan, D. H. Characterization and Application of a DNA Aptamer Binding to L-Tryptophan. *Analyst* **2011**, *136*, 577–585.